A Dissertation on

STUDY AND DETECTION OF MUONS USING RPC DETECTORS READ-OUT WITH NINO ASIC CHIP BASED BOARD

Submitted in the partial fulfillment of the requirements of the degree of

MASTER OF TECHNOLOGY

In

NUCLEAR SCIENCE & ENGINEERING

By

NISHAT AHMAD

2K14/NSE/18

Under the Guidance of

Prof. S. C. Sharma

(Supervisor)

&

Dr. Md. Naimuddin

(Joint-Supervisor)

Department of Applied Physics,

Delhi Technological University

(Formerly Delhi college of Engineering)

Govt. of NCT of Delhi

Main Bawana Road, Delhi-110042

YEAR: 2016

DECLARATION

I declare that this written submission represents my ideas in my own words and where others' ideas or words have been included, I have adequately cited and referenced the original sources. I also declare that I have adhered to all principles of academic honesty and integrity and have not misrepresented or fabricated or falsified any idea/data/fact/source in my submission. I understand that any violation of the above will be cause for disciplinary action by the Institute and can also evoke penal action from the sources which have thus not been properly cited or from whom proper permission has not been taken when needed.

PLACE:

DATE:

NISHAT AHMAD

(2K14/NSE/18)

ACKNOWLEDGEMENT

I wish to place on record my deep sense of gratitude to Dr. Md. Naimuddin, Assistant Professor from Department of Physics and Astrophysics, University of Delhi, Delhi for his initiative, encouragement and determination to help me. Had I not met him, my dream of doing a quality Master project, would have possibly remained a dream. My supervisor Prof. S. C. Sharma, Head of Department of Applied Physics, Delhi Technological University, Delhi is a lot more than just a professor to me. His teachings and the way he continues to lead experimental projects with deep commitment and involvement is inspiring a lot of us.

I am thankful to my Research Committee member Dr. Ashok Kumar, Assistant Professor from Department of Physics and Astrophysics, University of Delhi, Delhi for his valuable help and guidance. Thanks are also due to the faculty of my post graduate courses, my thesis referees and examiners.

I am grateful to the Department of Physics and Astrophysics Physics, University of Delhi, Delhi and Applied Physics Department of Delhi Technological University, Delhi for providing me with all the facilities required for carrying out this research work. I am grateful to Dr. Nitin K. Puri, Assistant Professor from Department of Applied Physics, Delhi Technological University, Delhi for his constant support and motivation.

In a way, this work has resulted from an ongoing large collaborative effort to build a massive neutrino experiment in the country. I wish to acknowledge many crucial contributions made by my colleagues, in particular the detector and electronics R&D team members Ankit Gaur, Mohd. Rafik, Aman Poghat, Rizwan Ahmad, Ashique Shah. I thank all the members for their support.

I am proud of my family, my village, my childhood friends, my schools and colleges, my teachers and my classmates. I am indeed very fortunate to have received love and affection all throughout my childhood, school and college days from everyone I met.

NISHAT AHMAD

(2K14/NSE/18)

Abstract

Important developments have occurred newly in neutrino physics and neutrino astronomy. Oscillations of neutrinos, and the inferred evidence that neutrinos have mass, are likely to have far-reaching consequences. This discovery has come from the study of neutrinos from the Sun and those produced in interactions of cosmic rays with the earth's atmosphere. The ground-breaking Home stake Mine Neutrino Experiment in the USA, the gigantic Super-Kamiokande detector and the KamLAND detector in Japan, the Heavy-water detector at the Sudbury Neutrino Observatory in Canada, and a few other laboratories, together, have contributed in a very basic way to our information of neutrino properties and interactions. Encouraged by these discoveries and their implications for the future of particle physics, plans have been made world-wide, for new neutrino detectors, neutrino factories and long base-line neutrino experiments.

Indian scientists started initiating in atmospheric neutrino experiments. In fact, neutrinos produced by cosmic ray interactions in the earth's atmosphere were first detected in the deep mines of the Kolar Gold Fields (KGF) in south India in 1965. In order to revive underground neutrino experiments in India, a multi-institutional collaboration has been formed with the objective of creating an India-based Neutrino Observatory (INO).

Considering the physics possibilities and given the past experience at KGF, the INO collaboration has decided to build a magnetised Iron CALorimeter (ICAL) detector with Resistive Plate Chambers (RPCs) as the active detector elements. In the first phase of its operation, ICAL will be used for atmospheric neutrino physics with the aim of making precision measurements of the parameters related to neutrino oscillations. The detector will be magnetised to a field of about 1.3 T, enabling it to distinguish the positive and negative muons and thus identifying muon-type neutrino and anti-neutrino produced events separately. This will be useful for ICAL to provide an exciting possibility to determine the ordering of the neutrino mass levels. Finally, this detector can also be used as the far-detector of a futuristic long-base-line neutrino experiment ix using the neutrino beam from a neutrino factory. Good tracking, energy and time resolutions as well as charge identification of the detecting particles are the essential capabilities of this detector.

The ICAL experiment will need about 27,600 RPCs each of about 200 cm × 200 cm in area. RPCs are fast, planar, rugged and low-cost gas detectors which are being, and will be, used extensively in a number of high energy and astro-particle physics experiments. They find

applications for charged particle detection, time of flight, tracking and digital calorimetry due to their large signal amplitudes as well as excellent position and time resolutions. A dedicated R&D programme is currently underway to design, develop and characterise large area RPCs, ultimately leading to their large scale and low-cost production required for the ICAL detector. In essence, this thesis outlines the successful completion of designing, building and characterising large size RPCs, for the first time in India.

To begin with, we developed a large number of single gap glass RPCs of 30 cm × 30 cm in area, using the glass procured from local market, and studied their operation in the streamer mode (using a gas mixture of R134a : Isobutane : Argon in the ratio of 62 : 8 : 30). The results fined from the characterisation study of these chambers were reliable with those reported in the literature. However, we were faced with a grave problem as far as stability of their operation is concerned. They died of sudden aging when operated continuously. In order to understand this problem, we studied widely the glass, gas and other mechanism of the RPC detector using a number of different method. We then fabricated a large number of RPCs of 100 cm × 100 cm in area and operated them in the avalanche mode (using a gas mixture of R134a: Isobutane: SF6 in the ratio of 95.15: 4.51: 0.34), without facing any aging problems. These chambers show typical efficiencies of over 98% and timing resolutions of about 1 ns.

For the full utilization of the outstanding timing properties of the Resistive Plate Chamber (RPC), front-end electronics with unique characteristics are required. These are (1) Differential input, to profit from the differential signal from the RPC (2) A fast amplifier with less than 1 Nano-second peaking time and (3) Input charge measurement by Time- Over-Threshold (TOT) for slewing correction. An 8-channel amplifier and discriminator chip has been developed to match these necessities. This is the NINO ASIC, fabricated with 0:25 mm CMOS technology. The power requirement at 27 mW/channel is low. Results on the performance of the RPCs using the NINO ASIC are presented. Typical time resolutions of the RPC system are in the 50 Pico-second range, with an efficiency of 99:9%.

The time over threshold method is used in the NINO amplifier chip in time of flight measurements in the MPD detector. For the TOF measurements MRPC detectors are used. Using a signal and noise generator the effects of the noise on the time resolution in the time over threshold method is experimentally studied.

CONTENTS

List of Figures

List of Tables

CHAPTER 1

INTRODUCTION

1.1 INDIA BASED NEUTRINO OBSERVATORY (INO):

The India-based Neutrino Observatory (INO) Project is a multi-institutional attempt expected at to building a world-class underground laboratory with a rock cover of approximate 1200 meters for non accelerator based nuclear physics and high energy physics research in India.

The project includes are as follows:-

(1) The construction of an underground laboratory and allied surface facilities at Pottipuram in Bodi West Hills of Theni District of Tamil Nadu,

(2) The setting of an Iron Calorimeter (ICAL) detector for the studying neutrinos, consisting of 50,000 tons of magnetized iron plates arranged in stacks with gaps in between where Resistive Plate Chambers (RPCs) would be install as active detectors medium, the total number of 2 m metres X 2 m RPCs being around 27,600 and

(3) The constructing up of National Centre for the High Energy Physics at Madurai Tamil Nadu, for the maintenance and operation of the underground laboratory, Human resource and development of detector R&D along with their applications. The underground laboratory, includes of a large cavern of size 132 m X 26 m X 20 m and some minor caverns, will be accessed by a 2100 meters long and 7.5 meters wide tunnel.

The primary aim of INO is to study neutrinos. Neutrinos are fundamental particles belongs to the lepton family. They appear in three flavours, first associated with electrons and the others with their heavier cousins the muon neutrino and the Tau neutrino. According to the standard model of particle physics, these particles are mass less . However latest experiments conclude that these charge-neutral fundamental-particles, have finite but less mass which is not known. They

oscillate between flavours as they propagate. Determination of the neutrino masses and their mixing parameters is the most important problems in physics today. The ICAL detector is designed to deal with some of these key problems in a unique way. Over the decade this underground facility is likely to develop into a full-fledged underground laboratory for latest studies in physics, biology, geology, hydrology etc.

The objective of INO is to carry out basic research on the fundamental particle called neutrino. Presently Twenty one research institutes, Universities and IITs are involved in this project. INO is likely to galvanise interest in fundamental science research in all over the country and particularly at Theni and Madurai districts of Tamil Nadu.The student of science across the country will have chance to pursue research in the field of particle physics and high energy physics while being located in our country. The laboratory will be located underground so as to provide sufficient shielding to the detector from cosmic background radiation. The construction of tunnel is very common and will not have any impact on our environment, water sources or dams in the region. The project have all the necessary clearances certificate from different Central and State Government authorities. A complete geotechnical studies was also approved out by the (GSI) Geological Survey of India.

The operation of INO will have no discharge of radioactive or toxic substances. It is not a weapons or defence laboratory and will have no planned or defence applications. Some sections of media in the recent have reported that the INO underground observatory and the tunnels is used for storing radioactive or toxic waste. Such reports are not realistic and are groundless. Department of Atomic Energy strongly refutes such wrong and nasty reports. It positively states that no radioactive waste will be reserve there at every time and INO will be used only for the reason of basic science research in the area of neutrino physics and high energy physics.

1.2 IRON CALORIMETER (ICAL):

The ICAL is a 50 kilo tones magnetized detector which is used to detect neutrino interactions that is induced by the atmospheric neutrinos. In the future, it may also known as a distance detector for a Neutrino Factory (NF) in an extensive baseline experiment. The detector is very well tuned to determine muon momentum produced in the CC $\nu\mu$ interactions. It is also able of detecting hadron showers formed in Charge Current CC neutrino interactions. INO has been

designed to set up an underground observatory in India to learn atmospheric neutrinos. INO will host a 50 kilo tons magnetized Iron CALorimeter (ICAL) detector consists of three modules, each of dimension 16 m x 16 m x 14.5 m. Total detector will be a stack of 151 horizontal parallel layers of 5.6 cm thick iron slab furnish within 4 cm gap for the active detector medium element.Resistive Plate Chambers (RPCs) of dimension 2 m x 2 m will be used as active medium part of the detector. Atmospheric neutrino interaction with the iron target will able to formed the muons along with shower of hadrons during a Charge-Current CC interaction process. ICAL detector will be capable to detect muons by using their extended tracks and hadron showers hits formed by neutrino events. ICAL will have a unique ability to detect the charge of the formed muon by its magnetic field which is approx 1.5 Tesla and hence can calculate the charge of neutrino. Since the neutrinos and the anti-neutrinos interact uniquely with matter, the atmospheric neutrinos with huge experience of flight distance can disclose the mass hierarchy problem while crossing through earth matter. Thus, ICAL with atmospheric neutrino source have a probable to solve the unidentified accurate mass spectrum of neutrinos.

Primary Aim of the ICAL

The primary physics aim for the ICAL are as follows below.

A. Determine the neutrino mass hierarchy.

B. Formulate precision measurements of the parameters, sin2 θ23 and $|\Delta m^2\ 32|$.

C. Study of Charge Parity violation in the neutrino sector and test of CP and Time reversal invariance.

D. Observation of the Non-Standard Neutrino Interactions (NSI).

E. Check the sterile neutrino oscillation hypothesis.

F. Study of the high energy cosmic muons and to find out the ratio of the numbers μ − and μ +.

1.3 THE RESISTIVE PLATE CHAMBER (RPCs):

The Resistive Plate Chamber is the heart of the ICAL detector. It is a gaseous detector, based on the principle of ionization of gas through charged particles. The RPCs were first developed in 1981 by R. Santonico and R. Cardrelli to modify and overcome the process of Planar Spark Chambers. The RPCs are easy and cheap to construct and propose a robust operation. The RPCs have large output signals and satisfactory timing resolutions. They deliver special resolution of a few centimeter. Nevertheless extreme simplifications were introduced in its realization. These incorporated absence of high pressure gas, less requirements of mechanical precision and exercise of plastic materials as a substitute of glass. The resulting detector, was found to be free from damaging discharges by construction and provided a time resolution of the order of 1 ns. Together these qualities made RPCs of prospective interest in a different and comprehensive range of applications in current experiments. In particular it has placed the option for plastic scintillators, based on cost considerations, whenever wide detecting areas are required in less counting rate environments. All these characteristics make them a enviable way for the ICAL detector.

1.4 NINO ASIC CHIP:

A low power and ultr fast front-end amplifier/discriminator Application-Specific Integrated Circuit (ASIC) chip NINO was developed for employ in the A Large ion Collider Experiment (ALICE) Time-Of-Flight. This is so-called NINO ASIC permits for an 8-channel input signal charge measurement by encoding discriminator pulse width with best timing resolution at very high rate, while at the similar time providing a very minimum noise performance and less power consumption characteristics each channel. NINO ASIC was developed by the LAA project at the CERN and is used for time-of-flight(TOF) measurements for particle apex modernization in the ALICE experiment of the LHC collider.

The chip has eight channels. Per channel is designed with an amplifier with less than 1 nano-second peaking time, a discriminator with a least detection threshold of 10 fs and an output stage. The output pulse has least time jitter (less than 25 ps) on the front edge, and the pulse width is reliant of the input signal charge. Each channel feeds 27mW, and the eight channels well

fit in a $2\times4mm^2$ ASIC process in IBM 0.2μm Complementary metal-oxide semiconductor (CMOS) technology.

Table 1.1 NINO CHIP SPECIFICATIONS

Parameter	Value
Peaking Time	1ns
Linear Dynamic Range	0 to 10 fC
Saturation Level	>100fC
Noise (with detector)	<5000 e-rms
Front edge time jitter	<25 ps rms
Power Consumption	27 mW/ch
Discriminator Threshold	10fC to 100fC
Differential Input impedance	40 Ω < Zin < 75Ω
Output interface	LVDS

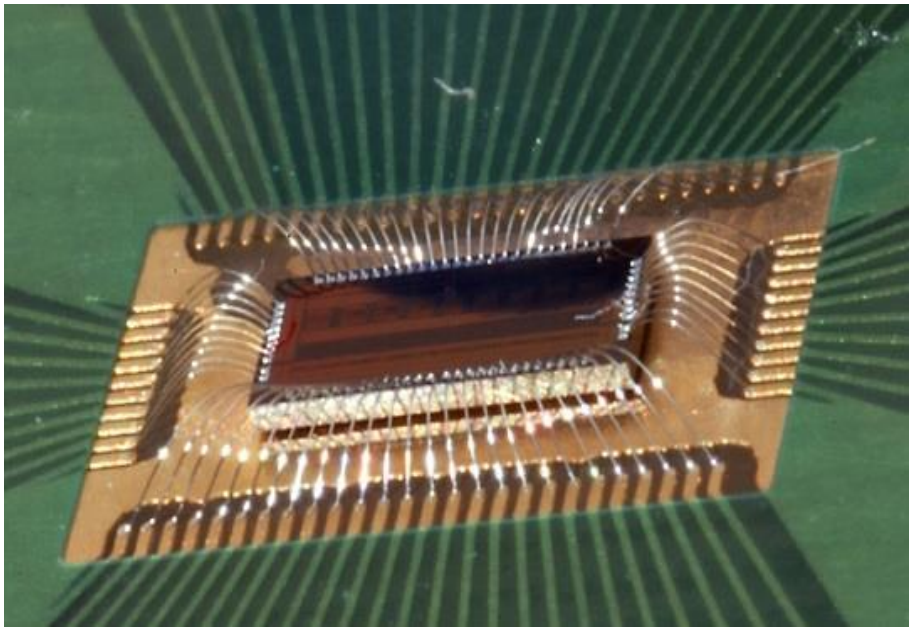

Fig 1.1 NINO ASIC Chip

CHAPTER 2

REVIEW OF LITERATURE

2.1 NEUTRINO:

According to the theory of Big Bang, neutrinos were born something like 15 billion years ago - soon once the birth of the universe and are now the most abundant particles in the universe after only to photons. However, theoretically neutrinos were proposed in 1929 by theoretical physicist Wolfgang Pauli to explain nuclear β decay. Early studies of β decay, discovered a continuous energy spectrum, distinct a discrete energy spectra observed in a two bodies radioactive decay. As constant search failed to detect the third particle, **Niels** Henrik David **Bohr** had even begun to study abandoning the theory of energy conservation in nuclear processes. Pauli postulated that an unobserved neutral particle that was escaping detection could take away the observed variation between the energy and momentum of the primary and absolute particles. The name neutrino is due to physicist Enrico Fermi, who, in 1934 took the neutrino idea seriously, and proposed a vital theory of weak interactions.

Bethe and Rudolf Peierls in 1934 used Fermi's theory to explain that the interaction cross section of neutrinos and matter would be about twenty orders of magnitude lesser than classic nuclear cross sections (~barns) and hence explained: "there is no experimentally possible technique of observing the neutrino". But, in a succession of practicle in 1956, The Frederick Reines and The Clyde Cowan finally proved their existence throughout the inverse β decay weak interaction process where an electron type anti-neutrino, νe formed in a nuclear reactor is captured by a proton p providing rise to a positron e+ and a neutron n.

$$\nu_e + p \rightarrow e^+ + n$$

Apart from electron-type neutrinos which are formed in nuclear β decay, the separate character of *muon-type* neutrinos was explained in 1962 by Leon Lederman et al by first observing interactions of the muon neutrino. When an other third type of charged lepton, the tau, was revealed in 1975 at the Stanford Linear Accelerator, it too was anticipated to have an associated neutrino. First indication for this third neutrino type came from the detection of absent energy

and momentum in tau decays analogous to the β decay. The first most observation of tau neutrino in 2000 by the DONuT collaboration, made it the most recent particle of Standard Model to have been straightly observed. A result of elementary importance to neutrino physics is the specific measurement of the decay size of the Z-boson which is saturated by (and hence indicates the subsistence of only) three active dynamic light neutrino flavours with masses lower than half the Z-boson mass. The subsistence of sterile neutrinos which don't involve in the weak interaction but which could be produced through flavour oscillation cannot be lined out from these measurements.

2.1.1 NEUTRINO ACCORDING TO STANDARD MODEL:

The Standard Model is a regular structure that embodies all of our recent understanding of elementary particles and forces, except gravity. It describes the way elementary particles interact. The Standard Model(SM) that incorporate 12 building blocks of matter (Fermions) - 6 leptons and 6 quarks, and their antiparticles all along with 4 force carriers (Bosons). The fermions are also mixed into generations. In general, fermion masses raise with generation.

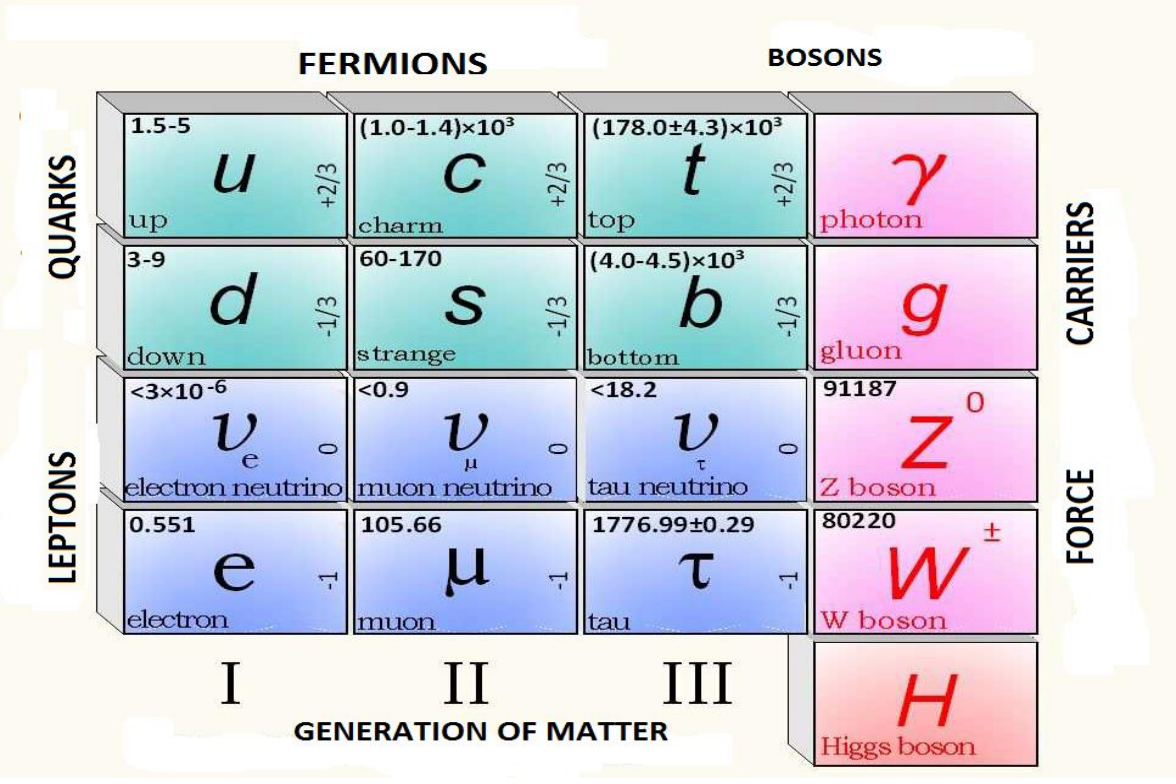

Fig 2.1 Generation of Matter

Above figure shows Standard Model of Particle Physics showing the electric charge (right) and mass for each of the particle in MeV (top left corner).

The quarks have partial charge and interact mostly through the color force, though they experience all further basic interactions. Their binding through the color interaction is what gives increase to the proton, the neutron and all the other hadrons. Charged leptons do not interact through the color force, but can experience the electromagnetic and feeble force. All matter and energy interact by gravity, however. Although we don't have a quantum law of gravitation, string theory holds assure of not only the quantizing gravity but also it unifying all four fundamental basic interactions. The other building blocks of Standard Model (SM) are the gauge bosons, namely, the gluons, the photons and the W-boson and the Z-boson that arbitrate the different interactions. In the Standard Model of fundamental particles attain mass by interacting with the Higgs field. The Higgs boson is discovered and its discovery is the major objective of the Large Hadrons Collider (LHC) experiments. In the Standard Model, the three neutrinos (and their anti-particles) are massless. Neutrinos interact with matter only by the weak force. It is accurately this lack of interaction potential that makes the neutrinos practically indefinable. According to the Standard Model, an electron neutrino cannot change to neutrino from another family as the lepton flavour number is preserved. Since the predictions of Standard Model have stood up till date to increasingly exact tests in observatory experiments, the study of neutrino mass and oscillation turned out to be a primary issue of neutrino physics and to the Standard Model as well.

2.1.2 NEUTRINO OSCILLATIONS:

Many significant observations on neutrinos from numerous type experiments all fall in one line, if neutrinos have mass and the flavors of neutrino states (electron, muon and tau) which contribute in the weak interactions are mixtures of mass Eigen states with special masses ($m_1, m_2 \ and \ m_3$). In common the two bases – flavor and mass states, are related by a unit matrix. The quantum mechanical development of the flavor states leads to the experience of neutrino oscillations, which was first explained by B. Pontecorvo. In fact, the idea of neutrino oscillations is entrenched in quantum mechanics. The neutrinos exchange identities, or oscillate into other flavours, as they circulate.

2.1.3 NEUTRINO PROPERTIES:

Neutrinos is only interacted by weak interaction. It is very hard to exclusively classify neutrino interactions along with the background of the cosmic rays interactions and an even radioactivity (depending on the neutrino energy). Neutrinos is all around travelling through matter, in general, are not easily observable because they do not hold an electric charge and therefore cannot ionize the matter. They do interact through the weak interaction in electric charge changing reactions (charged current (CC) interaction) or electric charge preserving reactions (neutral current (NC) interaction).

The subsistence of a neutrino mass robustly suggests the survival of a tiny neutrino magnetic moment of the sort of 10−19 Bohr magneton allowing the probability that neutrinos may interact electromagnetically as well

Experimental results shows that almost all neutrinos have left-handed helicities (spins anti parallel to momenta), and most of all anti neutrinos have right-handed helicities. In the massless limit, it shows that only one of the two possible helicities is experiential for either particle.

Earlier than the thought of neutrino oscillations placed up, it was commonly assumed that neutrinos travel at the velocity of light. However, for huge particles, this cannot be right. The neutrinos from the supernova were detected under the time window that was regular with a velocity of light for the neutrinos. So far, the problem of neutrino masses cannot be determined on measurements of the neutrino speed.

While the experimental results conclude that neutrinos have mass, their total mass scale is still unknown. It is due to the detail that neutrino oscillations are only sensitive to the difference in the squares of the masses.

In Astrophysics, neutrino is of technical interest because it can make an incomparable investigate for environments that are normally covered from the standpoint of other study techniques, such as optical observation and radio observation.

The first such as the use of neutrinos was projected for study of the core of the Sun. Direct optical study of the solar core is not possible due to the dispersion of electromagnetic radiation by the enormous quantity of matter adjoining the core. On the other hand, neutrinos generated in stellar fusion reactions at the core passes through the sun with little interaction. While photons

emitted by the stellar core may require a number of 40,000 years to disperse to the superficial layers of the Sun, neutrinos can virtually cross this distance at just about the velocity of light.

Neutrinos are also helpful for probing astrophysical sources away from our solar system. Neutrinos are the only known particles that are not extensively attenuated by their travel through the inter-solar medium. Optical photons can be covered or diffused by dust, gases, and the background radiation. High-energy cosmic rays, in the form of fast-moving protons and atomic nuclei, are not able to pass through more than about 100Mpc due to the Greisen–Zatsepin–Kuzmin (GZK) cutoff. Neutrinos can pass through this and larger distances with very small attenuation.

Another most important use of the neutrino is in the study of core collapse supernovae, the explosions that finish the lives of very massive stars. The core collapse phase of a supernova is an almost incredibly opaque and energetic event. It is so thick that no known particles are capable of escaping the advancing core front apart from for neutrinos. The usefulness of neutrinos as an investigate for this important event in the bereavement of a star cannot be overstated.

Neutrinos can also be used for researching quantum gravity effects. It is because they are not affected by either the electromagnetism and strong interaction or, and because they are not usually found in compound particles or flat to near immediate decay it might be possible to separate and calculate gravitational effects on neutrinos at a quantum level.

2.1.4 SOURCES OF NUTRINO:

The origins of naturally occurring neutrinos are both earthly and celestial. They are also produced using the particle accelerators and in nuclear reactors. Each of these sources provides information, rarely overlapping, that is extremely vital in understanding the essential properties of the neutrinos and its sources. The energy spectrum of naturally formed neutrinos begins from fractions of electron-volts (ev) and spans an impressive range.

Atmospheric neutrinos: Atmospheric neutrinos outcomes from the interaction of cosmic rays with atomic nuclei in our Earth's atmosphere, making showers of particles, a lot of which are uneven and produce neutrinos when it decay.

This process is represented by:

$$\pi \rightarrow \mu + \nu\mu \; ; \quad \mu \rightarrow e + \nu_e + \nu\mu$$

Atmospheric neutrino flux, which is roughly 103 per meter square per second, peaks just lesser than a GeV and fall after that quicker than $1/E^2$.

Big-Bang: Standard model of Big-Bang predicts, like for the photons, a cosmic background of the neutrinos. Even though they are very rich – about 330 neutrinos per cm^3, their energy is too small (about 0.0004 eV), that no experimentation has been able to detect them as yet.

Solar neutrinos: As per the Standard Solar Model, when four protons combine to become one helium nucleus, two of them have to change into neutrons, and each conversion releases one electron neutrino, which is directed by the following equation:

$$4p \rightarrow 4He + 2e^+ + 2\nu_e + 25MeV$$

Each and Every second, approx 65 billion stellar neutrinos surpass through every square of a centimeter on the Earth that faces to the Sun. While neutrinos are insignificantly fascinated by the mass of the Earth, the face surface area on the side of the Earth opposite to the Sun receives almost the equal number of neutrinos as the side facing to the Sun.

Supernovae: Most of the energy created in supernovae is radiated away in the form of a huge rupture of neutrinos. It is because neutrinos interact so small with matter, it is considered that a neutrino of supernova emissions transmit information about the innermost regions of the explosion. Second and important neutrino sources are the thermal energy of the lately formed neutron core, which is dissipated using the formation of neutrino and anti neutrino pairs of all the flavors. These processes can be represented by following equations. Approx neutrino flux studied from SN-1987a Supernova was 1012 per meter square per second.

$$p^+ \; e \rightarrow n + \nu_e \; ; \qquad e^+ + e^- \rightarrow \nu + \nu$$

Geologically produced neutrinos: Various of the isotopic constituent of earth are the naturally radioactive, particularly those with having half-lives of the order of the geological age. Neutrinos are produced as an effect of this type of natural radioactivity. In especially, the decay chains of Uranium-238 and Thorium-232 isotopes, plus Potassium-40, includes β decays which are accompanied by the release of anti-neutrinos and neutrinos. They can give information on the

interior of the Earth. The flux of the geologically formed neutrinos is about 5×10^{10}meter square per second.

Nuclear reactors: Nuclear reactors are the most important source of human-generated neutrinos. They have been the primary to be detected and also the initial to be used to put a number of limits on the neutrino oscillation. Anti-neutrinos are made in the β decay of neutron-rich offspring fragments in the process of fission. The process of standard nuclear fission releases roughly 200 MeV of energy, of which about 6 percent is radiated gone as anti-neutrinos. A standard nuclear reactor produces 2 × 1020 $\frac{v_e}{GWth}$ Nuclear bombs are also produced huge quantities of neutrinos.

Particle accelerators: Various particle accelerators have been used to create neutrino beams. The method is to crash protons into a set target, creating charged pions or kaons. These unstable particles are subsequently magnetically focused into an elongated tunnel where they decay while in travel. Because of the relativistic improve of the decaying particle the neutrinos are produced as a beam rather than isotropically. The lately built neutrino beam at the J-PARC accelerator observatory in Tokai, Japan is one such example. Efforts to build an accelerator facility where neutrinos are formed through muon decays are also continuing. Such a setup is known as a neutrino factory.

2.2 THE MAGNETISED IRON CALORIMETER:

The major focus of ICAL at INO is to learn interactions involving atmospheric *muon neutrinos and anti-neutrinos*. This needs the construction of a detector which is more sensitive to the energy, direction and sign of the electric charge of muons, created by charged-current (CC) interactions of neutrinos with the detector objects. This detector (perhaps advanced regarding fiducial volume) that will also be an appropriate option as a front-end detectors of the long-base-line experiment. Based on the physics aim of the ICAL detector, the following criteria was used for selecting an appropriate design for the detector system.

- A great target mass to attain a statistically significant number of the neutrino interactions in a sensible time-frame for the verification of atmospheric neutrino oscillation.

- To openly detect the oscillation pattern model in the L/E spectrum of atmospheric muon neutrinos, the energy E and the direction θ of the incoming neutrino have to be precisely measured in every event. The energy of the neutrino can be predicted by calculating the energies of muon and the hadrons produced in every event. The direction θ of the neutrino can be predicted from the direction of the muon formed from the ν_μ charged-current interaction. The energy and angular resolution of the detector should consequently be fine enough so that L/E can be calculated with an accuracy better than a half of the modulation stage.
- To approximate the distance traversed by the neutrino, it is required to set the flight direction (up vs down) of the muon produced by the neutrino with the high efficiency. A different method like increase of curvature in the magnetic field, many scattering along with the track or the measurement of timing in consecutive detector layers can be used to attain this. Of these, the time-of-flight(TOF) method is the most effective and allows the excellent up and down discrimination for a detector with a time resolution (σ) of 1 ns or better.
- Detection of the electric charge of muons so as to differentiate between the neutrino and anti-neutrino interactions. Charge determination is required to achieve mainly all of the physics goals explained above.
- Compactness, ease of construction and modularity which allows the possibility of phasing.

2.2.1 FUNDAMENTAL PARAMETERS:

The Iron Calorimeter detector with an intention mass of about 100 kilo-tons will be ideal to address the physics aims listed above. To start with they are proposing a detector of around 50-kilo tons, which may be distended to its last size of 100 kilo-tons in stages.A detector will have a modular composition of total lateral size 48 m $\times$ 16 m and will include of a stack of 151 parallel horizontal layers of 56 millimeter thick low-carbon iron plate interleaved with the 40 millimeter gaps to the house of the active detector layers. The height of the detector will be 14.5 meters. The ICAL detector will be divided into three modules of size 16 m $\times$ 16 m.

most important features of the ICAL detector and its active detector elements are summarised the table below:-

Table 2.1 Specifications of the ICAL detector and its active detector elements

ICAL Parameters	
No. of modules	3
One module dimensions	16 m × 16 m × 14.5 m
Complete detector dimensions	48 m × 16 m × 14.5 m
No. of iron layers	151
Iron plate thickness	56 mm
Gap for RPC trays	40 mm
Magnetic field	1.3T

RPC Parameters	
No. of RPC layers	150
RPC unit dimensions	1840 mm × 1840 mm × 24 mm
Readout strip width	30 mm
No. of RPC units/Road/Layer	8
No. of Roads/Layer/Module	8
No. of RPC units/Layer	192
Total no. of RPC units	28800
No. of electronic readout channels	3,686,400

The iron arrangement for this detector will be self-supporting with the layer over resting on the layer instantly below using steel spacers located every two meters along with the X-direction. This will create two meter wide roads along with the Y-direction for the placing of RPC trays. There will be a total number of eight roads each module in a layer. The particulars of the detector design are shown in Figure below.

Considering all over the size of apparatus and the huge active detector area of around 100,000 m^2, it is desirable that such a detector must be of cheap cost, modular structure in production with elements of a size appropriate for mass production on a time scale reliable with the necessity that the detector is globally competitive. This modular structure will permit untimely operation with the fulfilled modules while developing others.

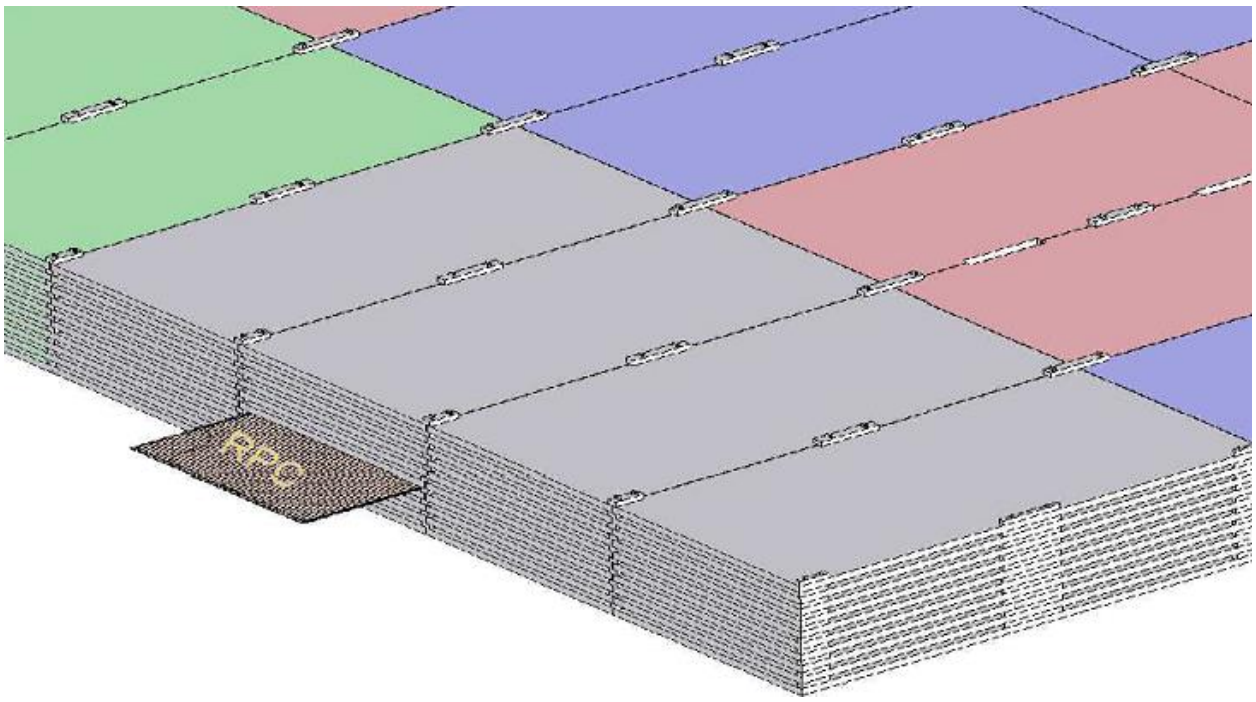

FIG 2.2 Schematic view of a part of the ICAL detector showing its constructional details along with an RPC.

The Magnet

The Iron Calorimeter magnet provides objective to nucleons for the neutrino interactions as well as it serve as a medium in which the secondary charged particles can be estranged on the basis of their magnetic inflexibility so that their momenta can be predicted. The magnetised iron calorimeter will include of about 50 kilo-tons of low-carbon iron. The carbon percent should be 0.1 percent or less in order to have a well magnetic characteristics.

The design process for the ICAL magnet are fundamentally the following:

Field uniformity: The performance of the detector will be the best when the magnetic field is uniform. We adopt a gap-less toroidal design for the magnet. In this design the magnetic field is mainly inside the iron and field leakage outside is minimum.

Field orientation: The least number of changes in the field orientation will be the criterion to be resolute by simulation and the event reconstruction.

Modularity: Even in the fundamental design with 50 kilo-tons of iron, the detector, and the magnet will be finished in three modules. The modules can be added at any phase later, either individually or in the pairs.

Optimum copper-vs-iron ratio: The copper to the iron ratio decide the price and the electrical power consumption. If we take a better ratio, then the power consumption is small resulting in lesser running cost but higher fixed cost. The heat dissipation in the coil depends on upon the volume of copper used. A little amount of copper reduce the copper cost but dissipates a huge amount of heat which has to be detached by using (LCW) low conductivity water flow throughout hollow copper conductors.

Access for maintenance: Modularity is of the main importance from the point of view of accessibility to give maintenance.

In the toroidal (gap-less) design, copper coil goes through two rectangular slots in the stack of iron plates. Four coils will be installed in the middle zone of the each detector module. The arrangement of the iron blocks with the coil slots in the ICAL magnet. The length, breadth and the positions of the slots are selected to produce a uniform field in as huge a volume of iron as probable. The design also facilitates simple insertion/removal of the active detector trays. The little cross-section of the copper conductor (10 mm $\times$ 10 mm) and the coil (625 mm $\times$ 80 mm) ensure the minor loss of fiducial volume of the detector. The coil dimensions are going to be massive 8 m $\times$ 14.5 m. We intend to use hollow copper conductors cooled by little conductivity water flowing through them. In addition, heat generates by the magnet coil can also be dissolute by conduction through the iron plates and by the radiation from iron surface.

A coil with forty thousand ampere-turns is required for producing a field of 1.3 Tesla in one module. We have used a three Dimensional commercial code MagNet 6.0 to design the magnet

and calculate the magnetic field. The difference of the field over the entire set of plates is likely to be within 0.3 percent, the field varying by less than 0.15 percent over a height of ± 5 meter from the centre. The variation of the field is quite consistent in the X-direction, varying by less than 0.25 percent but in the Y-direction it starts declining beyond the length of the coil slot (± 4 meter).

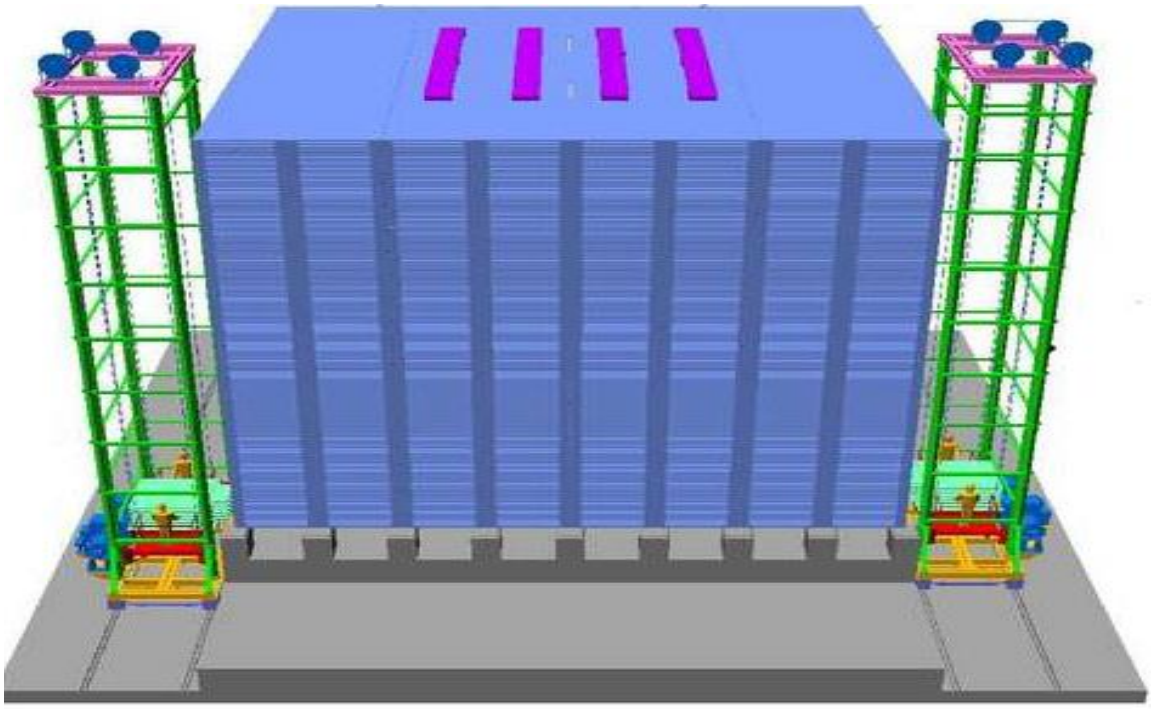

FIG 2.3 Schematic view of one of the three completed ICAL detector module along with the RPCs detector . The top view of magnet coils is also shown.

2.3 DETECTOR READOUT SYSTEM:

To attain the most important necessities of the ICAL detector readout system - time resolution of under 1 ns and the spatial resolution of superior to 1 cm for the detector, the Resistive Plate Chambers (RPCs) were selected as the active detector elements. Being planar in their mathematical geometry, RPCs are highly appropriate for detectors requiring big coverage. They are simple to construct using usually available materials, rugged, amenable for great scale industrial fabrication and simple to operate over long periods of time - all of which are extremely

desirable in case of ICAL detector. While the RPCs can be fabricated using bakelite or glass as electrode materials, we have at present opted for glass mainly because it is readily available in the local industry, has a good surface finish and less expensive.

The fundamental RPC detector elements for ICAL will be 1.84 meters in length and 1.84 meters wide. Eight such elements will wrap a road of 16 m$\times$ 2 m. A total of 28,800 elements, therefore, will be required to absolute the entire detector. The readout of the RPCs will be performed by outer orthogonal pick-up strips of 30 mm in pitch. The table summarises the stipulation of the ICAL detector and the RPC elements.

An enthusiastic R&D programme was started by the INO collaboration to design and fabricate big area glass RPCs. This work along with complete description of the RPCs, forms the topic of this thesis report.

2.3.1 RESISTIVE PLATE CHAMBER:

The Resistive Plate Chamber (RPC) was introduce by R. Santonico and R. Cardarelli in 1981 as a realistic substitute to the remarkably localized discharge spark counters, which finally achieved a time resolution of 25 ps. RPC is based on essentially the equal principle as that of the Pestov's Planar Spark Chamber. However radical simplifications were introduced in its realization. These incorporated lack of high-pressure gas, lesser requirements of mechanical precision and use of plastic materials in its place of glass. The ensuing detector was found to be free from destructive discharges by building and provided a time resolution of the order of 1 ns. Together these qualities made RPCs of potential interest in a diverse and larger range of applications in modern experiments. In exacting it has replaced plastic scintillators, based on cost considerations, whenever huge detecting areas are required in low including rate environments.

RPC is the particle detector utilizing a constant electric field formed by two parallel electrode plates, at least one of which is prepared from a material with the high bulk resistivity. A gas mixture with the high absorption co-efficient for ultraviolet light passes through the gap in between the electrodes. Whenever the gas is ionised by a charged particle passing the chamber, free charge carriers so as to deposited in the gap gas trigger the avalanches of electrons in the externally apply an electric field and create a discharge. Because of the high resistivity of the electrodes, and the electric field is suddenly losing in a limited area about the point where the

discharge originate. Thus the discharge is barred from propagating through the whole gas volume. The sensitivity of the counter remains unchanged outside this small region. On the other hand, due to UV absorbing component of the gas mixture, the photons formed by the discharge are not permitted to propagate in the gas. This avoids secondary discharges from forming at other points of the detector. The propagation of the increasing number of electrons induces a current on the external strip electrodes.

RPCs show much better time resolution than the wire chambers or the limited streamer tubes. This is a clear advantage arising from the uniform field as different to the 1/r field in the wire chambers, which imply large time fluctuations due to the drift motion of the electron. Very complicated versions of RPCs are being built lately, in which very flat electrodes of semi-conducting glass and huge pressure gas were utilised. These detectors provide time resolutions significantly better even than those possible by scintillators and quick photomultipliers.

2.3.2 BASIC PRINCIPLE OF OPERATION:

The job of a detector system in common is to recognize and to gauge the momenta and energies of the different particles, which depart their signatures in the detectors. The process upon which some gas detector is based is ionisation: the way of a charged particle through a gas volume gives increase to the formation of electron-ion pairs. The electrons drift velocity is much superior compared to that of ions. Considering a strong enough electric field is applied all through the gas volumes then the main electrons creates further ionisations. This growth mechanism consequence in a distribution of free charge in the gas which has the characteristics shape of an avalanche. Recombination processes frequently take place during the avalanche growth. Photons are formed in such as a recombination and they can in turn initiate the development of secondary avalanches. These are mostly produced along the axis of the primary avalanche. The command in which some secondary avalanches are produced causing huge amounts of free charge in the gas is called streamer regime. Further more, if the ion electron plasma is so bulky as to attach the two electrodes, then the so called the spark is formed. The propagation of the increasing number of the charges induces a signal on a read-out electrode.

The RPC detector in its easiest design is shown in Figure, two planar electrodes complete out of a resistive material (typically glass) having bulk resistivity of 1010 – 1012 cm are spaced by a

few millimeter. Other resistive materials such as melamine laminate with phenolic plates, cellulose, PVC, ABS etc. have also been used by developers. The electrodes are associated to a high voltage power supply in order to generate a consistent and intense electric field (about 5 kiloVolts/mm) in the gap between of them. A slim layer of graphite is coated over the above surface of the electrodes to allow uniform application of high voltage. The electrodes are kept separately by the means of little polycarbonate cylindrical spacers having a diameters of ~10 mmand a bulk resistivity greater than 1013 cm. A gas mixture including of Argon, Iso-butane and an electronegative gas like Freon (R134a). Argon acts as objective for ionising particles at the same time as Isobutane, being an organic gas, gives helps to absorb the photons that consequence from recombination processes thus limiting the configuration of secondary avalanches distant from the prime ones. An electronegative gas may serve up the reason of restraining the amount of free charge in the gas. This kind of gas mixture is mainly important when one wants to keep away from the onset of streamers. The surface resistivity of the graphite coating is too high enough to cause to be it transparent to the electric pulses formed by the charge dislocation in the gas gap. For these reason electric signals be able to be induced on metallic strips capacitive coupled to gap. The strips are mounted on the outer surface of the gap from which they are separated by a sheet of Mylar insulator. Two dissimilar sets of strips leaning in orthogonal directions may be set on both sides of the detector to get measurements in both planes. The strips act like transmission lines with classic characteristic impedance of around 50 ohm.

High resistivity of the electrodes avoids high voltage supply from providing the electric charge that would be required to keep the discharge between the electrodes. Therefore the electric field decreases drastically in the region of the discharge causing it to quench. This actions can be understood by studying that the typical duration of the discharge is 10 ns while the time constant (τ) with which the electrodes are recharged is not dependent of the detector surface dimensions and have of the order of ρ, where ρ and ϙ are resistivity and dielectric constant of the glass respectively. Assuming ρ = 5 $\times$ 1012 cm and ϙ = 4 $\times$ ϙ0 then τ $\approx$ 1.8 second.

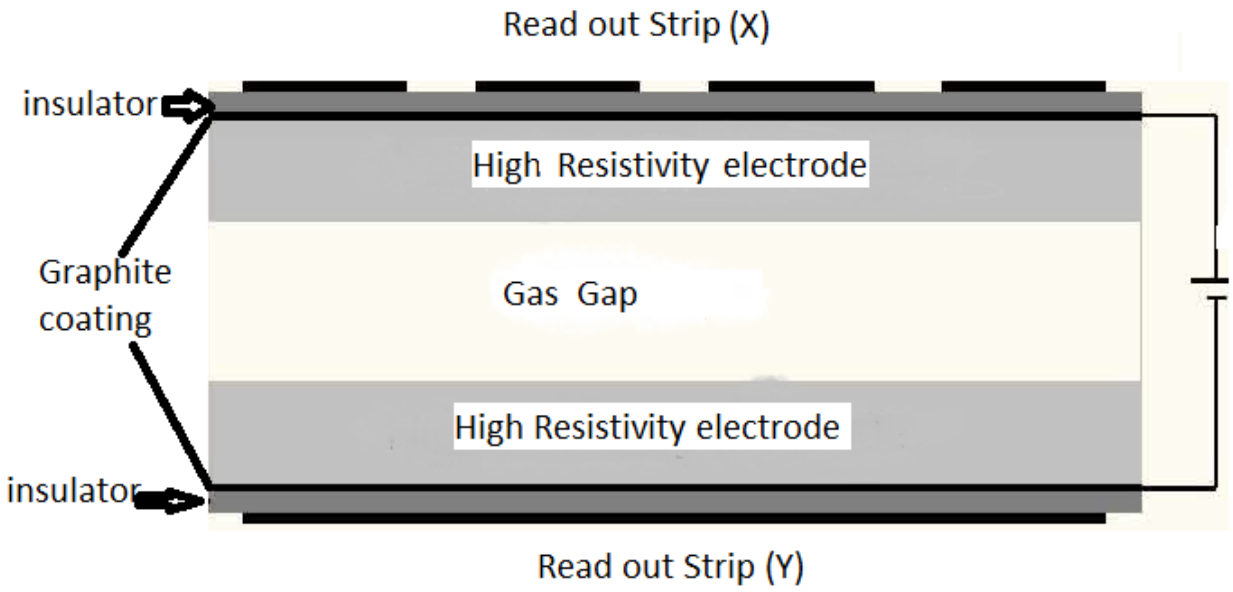

Fig 2.4 Schematic view of basic Resistive Plate Chamber.

The huge difference between τ and the typical discharge time in the detector inform that the electrodes act like insulators during the discharge. therefore only a limited area (typically about 0.1 cm^2) of their surface suffers from a high voltage fall. This area stays stationary for a time interval of order τ . This show that the detector dead time in the region of primary ionization. Counting rate capability of an RPC is governed by these quality times. Glass RPCs can therefore handle counting rates of up to around 500Hz/m^2 with a dead-time of less than 1 percent. Since classic bulk resistivity of bakelite is two orders of magnitude lesser than that of glass, the rate ability of bakelite RPCs is proportionately superior.

One would expect a easy explanation of the avalanche propagation in the RPC as the electric field pattern in the gas gap is very easy. However, it turns out that the physical processes are very compound. The detailed imitation of the time development of the signal requirements a dynamic computation of the electric field that is sensed by the electrons in the avalanche and that get contributions from the positive and negative avalanche charges. particularly at the final stage of the avalanche growth this space charge field can simply reach the similar strength as the applied electric field. At the two zones at the tip and at the tail of the electron distribution the total electric field is improved by the space charge field. At the middle of the avalanche, in the region

of greatest electron density, the total electric field is strongly fall down. This space charge effect is schematically as shown in Figure. For avalanches impending 108 electrons (the Rather limit), the high-field regions create the conditions for the growth of the cathode and anode (backward and forward) streamers, while the minor field region causes the decrease of gas gain seen by the avalanche. Both phenomena - avalanche saturation and streamers, share the common physical source and are typically concurrently present.

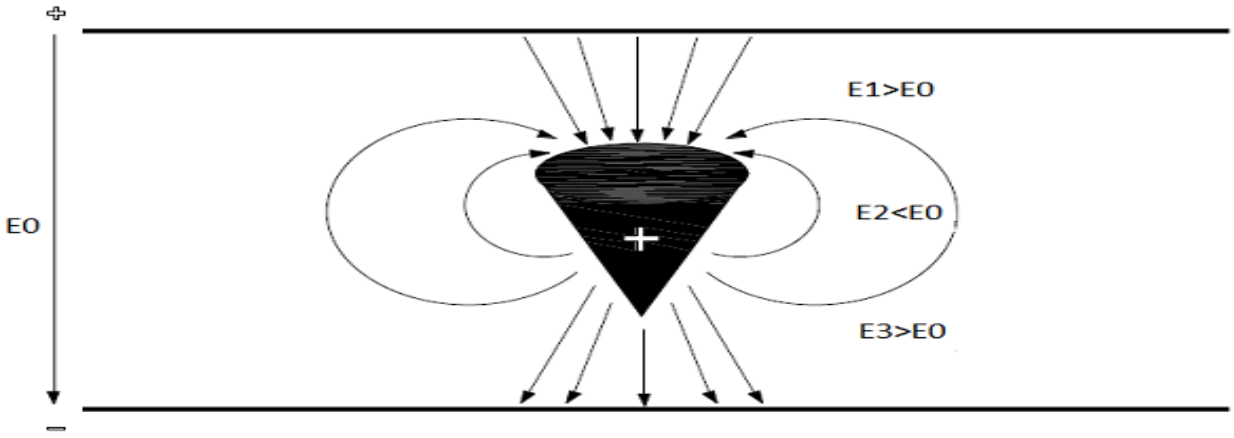

Figure 6: Schematic of an avalanche and the electric field variations cause by the avalanche charge carriers inside the RPC. E0 is the uniform field applied across the electrodes. E1, E2 and E3 are the effective fields at the tip, centre and tail of the avalanche charge distribution respectively.

Even although RPCs are being developed, deliberate and deployed for around three decades, there are still disagreements about the explanation of numerous aspects of their performance. Since the preface of timing RPCs with gas gaps of a few 100 microns and very high applied field strengths (~100 kV/cm), a seeming disagreement between the high efficiencies of the device and the rather small measured signal charges was experiential. To clarify the observed detection efficiencies, a huge density of main clusters in the used gases is essential, which contradicts experimental values. A large Ionisation density provides a higher possibility for the traversing particles to make electrons close to the cathode. The avalanches then travel approximately the whole gas gap (cathode to anode) and can thus attain sufficient sizes to pass the detection threshold. Yet in the case of a large ionisation density, the gas gain has to be very large to amplify the number of avalanches that over cross the threshold and thus explain the experiential efficiencies. This arise other questions: considering exponential increase of the avalanches, the

average avalanche charge would be up to 7 orders of magnitude better than the measured values. A extremely strong space charge effect is essential to clarify the small experiential charges of around 1 pC and an avalanche might not progress under such great conditions without rising into a streamer. Another difference concerns the shape of the charge spectra. Even as the statistics of avalanche growth predicts a shape following a power law, measurements demonstrate a peak that becomes additional pronounced at higher voltages.

2.4 OPERATING MODULES:

RPCs can be operated in the avalanche mode (also called as the limited proportional mode) or in the streamer mode. In the avalanche mode, the discharge of the primary charge by the arriving ionising radiation is followed by the propagation and the multiplication of the electrons matching to a Townsend avalanche. At a huge gas gain a vary occurs in the avalanche dynamics. Then the avalanche charge carriers power the electric field in the gas gap and therefore their own propagation and multiplication. This is so called the space charge effect. When the gas gain is improved further, photons begin to contribute to the propagation of the avalanche and streamers come into view. At a later phase, a conductive channel is created between the two electrodes, through which the confined electrode surfaces are discharged. A feeble spark may be formed. Even as in the avalanche mode RPCs streamers are an surplus side effect, streamer mode RPCs create use of the huge current pulses induced by the streamers which easily simplifies the read out of the tool.

The configuration of the electric signal in the RPC is basically based on the process of electron multiplication. Subsequent the way of an ionising particle through its gas gap, a certain number of main electrons are formed; they are arranged into clusters each of which is formed by a single ionisation. The n_0 electrons of a known cluster are accelerated by the electric field and start the growth in the gas. This procedure is characterized by the parameter α (first Townsend coefficient), which represent the number of ionisations per unit length, and by β which is the accessory coefficient, that is the number of electrons that are capture by gas per unit length. The parameter β become mainly important in the presence of electronegative gases. If x is the distance between the anode and the position where the cluster is formed then the number of electrons that attain the anode will be given by

$$n = n_0 e^{nx}$$

where,

$$\mathbf{n} = \alpha - \beta$$

The gain factor of the detector therefore is defined as:

$$M = n/n_0$$

Operating mode of the RPCs - avalanche or streamer, be able to be illustrious by the value of M. If M is larger than 108, then main ionisations will give increase to streamers with high possibility. On the contrary values of M much lesser than 108 are small enough to prevent formation of extra secondary avalanches and the easy charge increase phenomenon occurs. In this case lesser amounts of charge are formed and the detector is supposed to operate in avalanche regime. Transition into streamer mode by an RPC intended to operate in the avalanche mode is frequently a severe trouble to deal with. This was shown to depend both on the preliminary electric field (set up by the bias voltage) as well as by the field produced by prime avalanche.

As recommended by Y.N. Pestov, a planar detector with resistive electrodes can be model as a place of discharge cells which to the first order can be considered as not dependent of each other. The easy expression of the capacitance of a planar condenser leads to the result that the area of such cells is relative to the total average charge Q that is formed in the gas gap.

$$S = Qd/\ 0V$$

Where, d is the gap thickness and V that is the voltage applied to the electrodes. This expression explain the vital role played by the parameter Q in the most detection rate that an RPC is able to maintain efficiently: the lesser the value of Q, the lesser the surface of the discharge cells and thus the higher the rate ability. The average charge formed in the gas gap for an RPC operating in the streamer mode is 100 pC, while in the avalanche mode the value is about 1 pC. Operation in the avalanche regime requires, however complicated front-end electronics. Indeed the essential idea in this regime is to move a large fraction of the gain factor characterising the

streamer mode from the gas gap to the front-end electronics. The later must offer large intensification factors and at the same time a huge bandwidth in order not to ruin the detector intrinsic time resolution.

2.4.1 AVALANCH MODE OF RPC:

The high rate application and detector aging issue complete the operation in avalanche mode trendy. This is achieved by considerable reduction of the charge formed in the gas gap. The counting rate ability of RPCs is enhanced by more than an order of magnitude if the incidence of streamers is concealed by working the detector in the avalanche mode. It was also facilitated by the growth of new highly quenching $C_2F_4H_2$-based gas mixture or with accumulation of minute fraction of SF_6 to the gas mixtures. The $C_2F_4H_2$ gas in exacting exhibits other outstanding features as like a fairly high density (resulting in high primary ionization) and a small operating voltage. Even as the physics of streamers is hard to study, the avalanche mode is agreeable for complete simulations of the physics processes in RPCs. graphic images of the development of an avalanche in an RPC and the electric field deformations cause by the avalanche charges at great gain are shown in Figure. E_0 is the applied consistent electric field across the gas gap. Some of the gas atoms are ionised by the way of a charged particle through the gas gap (top-left panel). The avalanche is started. The avalanche size is satisfactorily large to influence the electric field in the gas gap (top-right panel). Electrons reach the anode plate. The ions drift much slower due to their considerably lesser drift velocities (bottom-left panel). The ions reach the cathode. The charges in the resistive layers influence the field in a minute area around the position where the avalanche is urbanized (bottom-right panel).

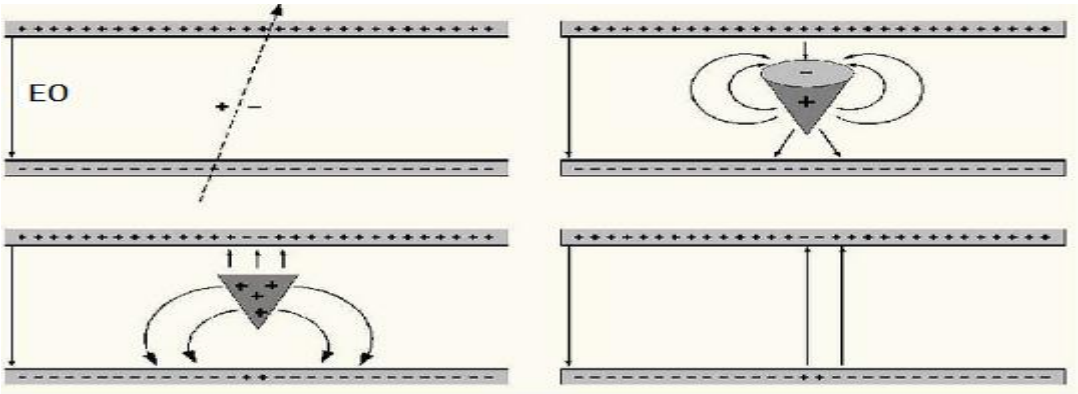

Fig 2.5 Schematic images of the development of avalanche in an RPC.

2.4.2 STREAMER MODE OF RPCs:

As the streamer signals are fairly great (between 50 pC and a few nC), no amplification is wanted and the signals be able to be discriminated against the detection threshold straightly.

Therefore the read out of streamer mode RPCs is quite straightforward. Double gap chambers operated at electric fields of 40 kilo-Volt/cm in streamer resime and with two mm wide gaps arrive at the efficiencies of 99 percent and a time resolution about 1 nanosecond. But, the rate ability is limited to a few 100 Hz/cm^2.

Graphic images representing different phases of development of a streamer in an RPC are shown in Figure. The top-left panel represents the development of an avalanche, as in case of avalanche mode shown by Figure. The avalanche charges lead to a high field distortion in the gas gap. Furthermore, high energetic photons create to contribute to the avalanche development and cause a fast spread of the avalanche: a streamer evolves (top-right panel). A feeble spark may also be formed at this phase. The local electrode area is discharged (bottom-left panel). Area is localised due to high bulk resistivity of electrode material. The electric field is strongly fall down around the mark where avalanche is produced. Detector develops a blind mark (bottom-right panel).

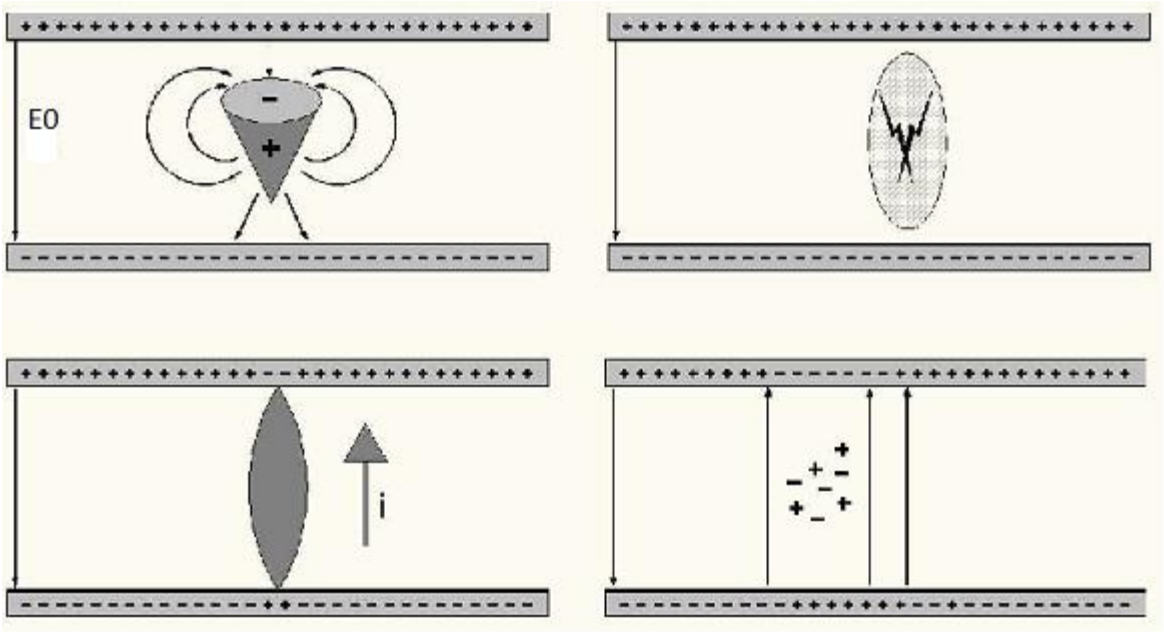

Fig 2.6 Schematic images of the development of streamer in an RPC .

2.5 DEVELOPMENT AND CHARACTERIZATION OF RPCs:

The INO group effort is planning to construct a massive 50 kilo-tone magnetised ICAL detector, to observe atmospheric neutrinos and to make accuracy measurements of the parameters associated to neutrino oscillations. Around 30,000 glass Resistive Plate Chambers (RPCs) of about 2 m × 2 m in size are going to be deployed as an active elements for the ICAL detector. An insistent R&D program to fabricate and characterise these great area glass RPCs was undertaken. Preliminary our work with chambers of 30 cm × 30 cm in size, we went on to make a large number of glass RPCs prototypes of 100 cm× 100 cm in size and had studied in detail, their performance and its long term stability. We have fundamentally finished the detector R&D programme for the ICAL detector recently by successfully fabricating and characterising 1 m × 1 m RPCs

We describe the design and development of two generations of RPCs along with their characterization and its performance results. We have put in strong efforts to indigenously develop and create a numbers of materials and components requisite for fabrication of RPCs. We have also designed and optimized a number of fabrication jigs and the quality control procedures for an assembling the gas gap.

We discuss these developments. One of the main problems we faced during this R&D work was the RPCs aging, while they were operated in the streamer mode. We will also emphasize this critical, but an issue yet to be totally comprehended.

2.6 OUR EARLY WORK AND RESULTS:

We initiated our RPC detector R&D by fabricating and testing chambers of 30 cm X 10 cm in area. The extremely first chamber was assembled without gluing, by using *E*-shaped spacers between the glass electrodes to make uniform gap between them. The chamber was not yet congested on sides. It was experienced by housing it within a drift chamber shell, through which gas was pass. The upgrade version was made by comparing an acrylic frame from a only sheet and gluing the glass electrodes inside the frame. The chamber is closed and the gas ports were shaped by laterally milling the external margins of the acrylic frame. These chambers did not work fine. The primary successful effort was when we built and operated some RPCs of 30 cm×

30 cm in size. We have used a numeral of materials which were provided by our collaborators and the other researchers during our early R&D work. But we have urbanized our first gas system, , data acquisition system, assembly jigs and the other facilities ourselves. We describe the work and the early results in the following sections are as

2.6.1 SMALL RPC DESIGN AND FABRICATION:

We have uses two mm thick standard Asahi float glass procured from the market in Delhi. We have selected float glass in excess of Bakelite due to its excellent surface consistency achieved without the surface treatment, resulting in improved field uniformity and thus fewer noisy operations. We found the normal deviation of the thickness measurements on two mm glass sheets using ultrasound thickness gauge to be fewer than twenty μ m. The glass sheets after crossing through mechanical and dimensional tolerance tests were cleaned of some likely oil deposits using liquid soap solution. The insulator spacers used for maintaining accurate and electrically isolated gap between the glass electrodes as well as the *T*-shaped frames used for sustaining support the electrodes and for forming an with this enclosed gas volume were made up of particular PVC material, brand named *NORYL*. We have used these materials of the design working in the Belle experiment. The spacers between the electrodes were set in staggered way in order to create the gas pass within the chamber uniform. The glass plates, the spacers, the frames, the gas inlet and outlet nozzles are all assembled by using a extraordinary 3MScotch-Weld 2216 or DP-190 epoxy. This glue was selected for its outstanding shear and peel-off strengths as well as its noble properties with the majority of the detector gases. The leak tests of the completed chambers were performed also by maintaining overpressure of around 20 mbar for gas tightness or by means of a hand-held Freon gas leak manager of model GH-202F. Chambers which show leaks of classically more than 10 ppm level are as re-glued.

The High voltage is applied across through the electrodes by the means of a semi-resistive coating. We devised the following process for coating the glass electrodes. We mixed a locally available dry colloidal graphite powder (of Grade 40019) and engineering lacquer in concerning 1 : 8 ratio by weight all along with thinner used for reliability. This mixture was sprayed regularly on the cleaned glass electrode surfaces using a standard paint spray gun normally used in the auto shop. We obtained a low, but regular, resistance of 100 - 200 $K\Omega$ using this technique.

The signal pick-up panels were prepared up of poly-isocyanurate foam board with unbreakable poly-aluminum foil facers on mutually sides. While on one the side of these materials, strips of required pitch was crushed the other surface was used as the ground orientation for the picked up signal. Mylar sheets were used for achieving the essential insulation between the RPC's electrode surfaces and the pickup strip panels which were mounted in get in touch with either side of the gas gap for the RPC operation process.

The Gas inlet and outlet ports were implemented by fabricating particular nozzles which have standard nipples for holding the plastic gas tube on one side, while the other side of the nozzle was hard-pressed flat to be capable to glide in between the electrodes of the chamber.

We fabricated a dozen small area chambers of dimension 30 cm $\times$ 30 cm. We also prepared a couple of large area chambers of dimension 100 cm $\times$ 100 cm. Design of the small and large area chambers was indistinguishable. We have urbanized a number of useful jigs and tools to determine the superiority of raw materials as well as a variety of fabrication phases of the glass RPCs. The jigs helped us in attaining velocity and consistency in the RPC manufacture. We have also standardised all the assembly events of the chambers. One of the premature small area prototype chambers is shown in Figure all along with a few of the RPC assembly jigs as developed locally.

2.7 GAS MIXTURES AND GAS SYSTEMS:

The option of a appropriate gas mixture for RPCs is runned by factors such as small working voltage, large gain, linearity and high rate ability. For a maximum working voltage, non-reactive gases are usually selected since they need the lowest electric field intensities for avalanche configuration. Because of thier higher precise ionisation and lesser cost, Argon is frequently preferred. But energized Argon atoms produced in the avalanche, de-excite emitting high energy photons. These photons are able of further ionizing the gases and causing cascaded avalanches, which is often unwanted. This trouble is usually solved by addition of polyatomic gases, such as Isobutane to the gas mixture. These molecules work as quenchers by absorbing the photons and then dissipating this energy during dissociation or super-elastic collision, where the kinetic energy of the two molecules in the last state is extra than that in the first state. The gas quenching can be increased further by adding up a sensible amount of electronegative gases such as Freon

(R134A is its eco-friendly replacement). These gases catch the boundless (to the electron cluster) but energetic electrons from the gas volume before they can start a new avalanche. Of late, SF_6 is being chosen to Freon, particularly if the avalanche resime of operation is preferred. It is also establish that the trouble of RPC aging which is recognized to be caused due to water vapour contagion in a Freon based gas mixture, is not experiential if SF_6 is used. We have used Freon, Isobutane and Argon gas mixture at the ratio of 62: 8: 30 by volume for the majority of our preliminary studies.

The gas mixing unit has the ability of mixing these 4 individual gas components and manage the mixed gas flow throughout the detector chambers and has been designed and developed with the assist of a local industry.

Fig 2.7 Gas Mixing Unit

The mixing unit has stipulation either to run the mixed gas directly into the detector chambers or to amass it in a pre-mix gas cylinder (15 liters in capacity) for a later use. We have used Rota meters for gas provision instead of more complicated mass flow meters in order to decrease the in general cost of the unit. Total details of the design and fabrication of this unit are given in

Section. A microcontroller based gas bubble counter was urbanized and mounted on the output gas line of the chamber for managing the gas flow rate through the chamber all along with a differential pressure gauge. During usual operation, just about one volume (of the chamber) change of gas per day is sufficient. We used steel tubing for gas supply lines from the gas mixing unit to the RPC test stand. We used standard Norton Tygon supple plastic tubes for small connections inside the test stand.

CHAPTER 3

REPORT ON PRESENT INVESTIGATIONS

3.1 RPC MATERIALS AND ITS ASSMBLY PROCEDURES:

RPC fabrication have includes deploying a huge number of materials also a lot of assembly procedures. So the manufacture of high performance and dependable chambers involves selecting the accurate type and quality of the materials as well as optimisation of a variety of assembly and quality control procedures concerned in the fabrication. The materials include of glass used for electrodes, individual gases are used for the mixing and flowing the gas mixtures for the procedure of the chambers, spacers, buttons, gas nozzles etc. which are required for the assembling the chamber, the resistive coat on the electrodes, epoxies used for cohering together various types of materials, pickup panels are used for exterior signal pickup from the chambers, polyester films are used for insulating the pickup panels from resistive coated electrodes, to name a little. We have deliberated a number of various types and qualities of these materials and optimized most of them. We have incessantly enhanced the quality of the RPCs by absorbing the results of these studies in the fabrication and the testing of chambers.

We have also construct and developed a huge number of assembly and quality control procedures and made-up a number of useful jigs that are tremendously useful in the fabrication of a good quality detector. A Coating of the resistive paint on the electrode, assembling and cohering of chamber, leak testing of the complete chambers are some of the significant assembly procedures. We have worked closely from **the Lab of RPC at University of Delhi, R&D** institutions in mounting these materials and designing and developing the assembly procedures.

3.1.1 GLASS ELECTRODE COATING:

The resistive coating of the external surfaces of the electrodes plays a very vital role in the procedure of the RPC detector. While the surface resistivity of this coating should be tiny enough so that the bias voltage that is compulsory for the RPC operation can be applied on these coats, it should be high enough to make it transparent to electric pulses generated by the charge displacement in the gas gap. This way, the charges are produced inside the gas gap on

passageway of a particle, can persuade electric signals on the external metallic pickup strips, which are capacitive coupled to the gap. There is another significant consideration of this electrode coat on the performance of the RPCs. Every charged particle passing through the RPC produces a tiny charge spot of about 0.1 cm^2in area. This area is very small to result in any obvious cross-talk between two adjacent pickup strips on which signals are induced. However, if the surface resistivity of the graphite coat is very small, the induced charge is less localised and spreads across the graphite coat, producing great cross-talks between the pickup strips and thus harshly affecting the position resolution of the detector. The cluster size of an RPC exponentially decreases with the surface resistivity of its electrode coating. The cluster size of 30 mm at a surface resistivity of 20k/A reduces to around 8 mm as the resistivity is improved to 1M/A. On the other hand, thin coats with surface resistivity of 0.1 - 1 M result in time constants that are analogous to the charge movement duration.

Fig 3.1 Glass Electrode

Needless to articulate that the uniformity of response across the RPC is reliant on the uniform resistivity of the coating across the surface of the electrodes. It is also significant (for the long term stability of the RPCs) that the binding strength of the coat to the electrodes is strong. Studies by G. Aiell have revealed that degradation of the anode graphite coating is one of the major factors for long-term aging of the RPC. In order to stop damage to the painted surfaced due to treatment; a thin insulating PET film is cohering on the painted surfaces. Lastly, the materials used, as well as the method employed, for coating should be flexible for large scale industrial production.

Other techniques such as metal oxide paints, anti-static paints, graphite varnishes, adhesive graphite foils special inks and commercial automobile paints are also used. We had started with a graphite paint prepared using colloidal grade graphite powder (3.4 gram), Duco-lacquer (25 gram) and Duco-thinner (40 ml) and sprayed on the glass electrodes by using an automobile spray gun. While the graphite powder of suitable grade provides the requisite surface resistivity, the lacquer binds the graphite to the smooth glass surface. A thinner is added to get the required uniformity of the mixture that permits spraying using a spray gun. A uniform graphite coat of stable surface resistivity (100−200 k/A) could be obtained by this technique. Shown in the left panel in Figure is a plot of the surface resistivity measurements of a painted glass for over a month. The surface resistivity of the coat drops quickly during the first few days of application, basically due to evaporation of the thinner from the coat, and remains sensibly stable thereafter. Even though this technique worked fine for the fast manufacture of small prototype RPCs, one of the problems using this technique was that the paint came unstuck from the glass with time and handling. The data is obtained with the help of an indigenously developed novel jig (shown in the right panel of Figure), which allows rapid measurements without causing harm to the painted surfaces. It works on the following principle: The resistance, "*R"* of a surface film of thickness, "*t"* as measured between 2 conductors of length, "*L"* and separated by width, "*W"* is proportional to $L/(W \times t)$. So for a given square of side, L (which is equivalent to W), R is not dependent of L (and W) and depends only inversely on t. The jig basically consists of 2 conducting bars fixed in frame so as to form a square. Stipulation is made to measure the resistance across these conducting bars, using a multimeter. The resistance value is directly read as k/A. The jig is purposely made heavy so that it makes good quality surface contact with coat and thus provides reliable measurements. Jigs of little and big squares were made-up so that the resistivity measurements on both fine and coarse length scales could be made.

Subsequently we urbanized a particular conductive paint in alliance with a local paint company. This paint uses customized acrylic resin as a folder, conductive black as pigment and aromatic hydrocarbons and alcohols as solvents. We have devise the following procedure for painting the glasses. We have establish that cleaning of the raw glass received from the factory, is a most significant factor for predictable performance and long-term operation of the RPCs. The glass plates are first cleaned using ethyl-alcohol and soak with distilled water. Then we apply a soap

solution (Labolene) on the glass sheets and clean those thoroughly using distilled water after soaking for around ten minutes. The spraying of paint is completed with a gun of nozzle size of 1.3 - 1.6 mm and at a pressure of around 4 kg/cm^2, maintaining the glass plate at a distance of around 15 - 25 cm from the gun. While at room temperature, the painted surface dries in about ten minutes, it takes about 18 hours for complete drying. The required surface resistivity could be collect by fine tuning the amount of thinner in the paint mixture.

Painting of vast number of large area RPCs using the physical method would be quite not practical and result in piece to piece variations in the surface resistivity or the thickness of the paint. Therefore we have developed an automatic system to paint the glasses with the assist of a local industry, a prototype of which is shown in the Figure. A basic scheme using infrared radiation for curing of the paint was also urbanized. Work is underway to manage both these systems, making them appropriate for the great scale production of painted glasses.

Detailed studies are done on the surface resistivity of the glass electrodes coated using the automatic plant. We used two jigs - 36 cm^2 and 1000 cm^2 in area, to measure the values for 2 ranges in coated areas and also took data insertion the jig in two orthogonal orientations in order to average the values obtained. Shown in Figure are contour plots of the resistivity obtained from 100 cm $\times$ 100 cm glass sheet in the two orientations of the jig. As can be seen from the plots, the measurements obtained are close to the design values and are uniform over the surface, except close to the edges.

3.1.2 DEVLOPMENT OF SPACERS, BUTTONS AND NOZZLES:

Resistive Plate Chambers are basically of a parallel plane geometry detectors. The chamber is constructed by mounting two glass electrodes of required area and thickness, parallel to each other and alienated exactly by the necessary gap between them. The chamber volume is realised by closing all the four edges of the above assembly with spacers of T-shaped cross-section. These detectors are constantly managed in a nonstop gas flow mode. So, the spacers used for closing the detector volume, the buttons used for maintaining the requisite gap and mechanical inflexibility as well as the gas nozzles required for leasing the gas in and out of the detector chamber are the mainly important components for fabrication of an RPC. We recognized and investigate a variety of materials as well as shaped a number of designs for these components

and advanced them. We then collaborated with a local industry and produced these components by using polycarbonate material.

As the spacers were produced by using a die, the buttons and gas nozzles were produced using injection molding process. All the requisite tooling was planned by us in coordination with the industrial fabricator. We have subjected the finished products through severe mechanical and other quality control tests. We have taken a significantly huge number of measurements on each dimension of these components and methodically analyzed the data as part of the quality control process. We have also made-up RPCs to reveal the suitability of these components in the RPC fabrication. This had necessary a few iterations in the fabrication phase before attaining the final products that meet our specifications. We have finally accomplish tolerances of 5-8 μm in various dimensions of the spacers, buttons and nozzles. We have used these indigenously developed components throughout in our on-going detector R&D programme. Figure shows from left to right, the theoretical designs of spacer, button and gas nozzles.

3.1.3 VACCUM JIG FOR RPC GAS GAP ASSEMBLY:

One of the mainly crucial aspects of fabricating the RPC gas gap is to mount the two glass electrodes parallel to each other. This assures a uniform field across the whole area of the chamber when high voltage is applied to the electrodes. As mentioned before, polycarbonate buttons are used to keep this specific gap between the electrodes. It is evenly important that these buttons are cohere perfectly on each sides to the electrodes so that they will give rigidity and mechanical potency required for the assembly to conquer the pressure exerted by the gas flowing throughout the chamber.

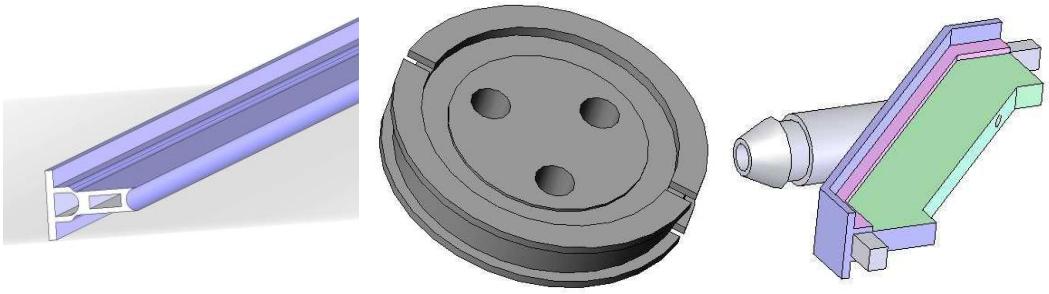

Fig 3.2 Conceptual designs of spacer (left panel), the button (middle panel) and the gas nozzle (right panel). Intricate details in the designs of these seemingly simple components may be noted. For example, different cut-outs and holes in the button design add to glue contact area with the glass sheets.

In order to attain the above aims, the following process is used. First, the bottom glass sheet is located on a completely even working platform. This platform itself is mounted on an unbending stand using ball bearings, such that it can create a complete rotation all around its axis. The accurate amount of glue is dispensed at the elected grid points on the glass, where the buttons are going to be located. The buttons are then positioned at these points. Glue is again applied on the upper side of the buttons and the top electrode glass is positioned on the buttons. The glass sheets are handled with help of a numerous suction cup assembly, which is anchored to and stimulated using a chain pulley block. In order that the buttons are cohere well on both sides to the glass electrodes, heavy metal or lead blocks are located at many places on the assembly. Though this method is widely used, it is not a appropriate for manufacture of large area chambers, because it is hard to apply uniform pressure across entire area of the chamber. We have therefore developed a very stylish and cheap jig to overcome this problem based on a novel method. This is depicted by Figure. four ports are provided on the RPC fabrication table, just outside the four corners of the chambers. These ports are connected in parallel using plastic pipes and connected to a specially designed bubbling jar. The glass jar has three pipes mounted using its cap a flange. One pipe of huge diameter is set in such a way that one of its ends is deep inside the jar and the other end is open to air. The pipe which is associated to the RPC fabrication table ports is set in such a way that one of its ends is inside the bubbler jar. Finally, the third tube is connected to a vacuum pump on one end while the other end is placed just below the cap of the bubbler jar. The jar is filled up with water in such as way that the huge pipe is in water and the water level of around 80 mm is maintained below the tube which is connected to the RPC fabrication table.

After the buttons are cohered to the glass sheets, the assembly is enclosed with a polythene sheet on the top and it is sealed to the table on all four sides. The vacuum pump is then switched ON. The pump first removes the air from the volume above the water level in the bubbler jar, followed by the air from the volume fashioned by the polythene sheet. As this procedure continues, the atmosphere exerts pressure on the polythene sheet, which in turn keeps the two glass electrodes firmly pressed against the buttons unraveling them. Meanwhile, while a low

pressure volume is generated over the water level, atmospheric pressure pushes the water level up in the bubbler jar till the top water level touches the lower end of the pipe, which is connected to the RPC fabrication table. From this stage onwards, the volume formed by the polythene sheet is not evacuated and the pump only runs now to stay the equilibrium pressure which was attain. This way the two glass sheets are held together tightly and parallel to each other, with the gap determined by the buttons. The pump is usually run for some hours, till the glue is totally set. After the two glass sheets are cohered together along with the buttons, the edge spacers and gas nozzle assemblies are glued on one side of the gas gap. When the glue sets on this side, the gap is rotated upside-down using the mechanism mentioned above, and the edges on the other side are glued. This simple jig was found to be an helpful tool for large area RPC gas gap fabrication and found to result in zero failures while fabrication.

3.1.4 DEVELOPMENT AND CHARACTERISATION OF PICKUP PANELS:

Pickup panels are mounted on the either side of the RPC detector volume. The charge produced in the gas volume due to passage of a charged particle through the chamber, induces signals on the strips of the pickup panels due to capacitive coupling. A well design of the pickup panel is vital not only in terms of its mechanical dimensions, but also in terms of its electrical properties. Pickup panels are usually designed using a dielectric medium between two metallic layers. The metallic layer facing the RPC detector volume is segmented as per the requisite spatial resolution from the chamber. As far as the mechanical properties are concerned, it is perfect to have the thin pickup panels so that the overall thickness of the finished chamber is minimized. On the other hand as far as the electrical properties are concerned, as it will be ideal to have the characteristic impedance of the strips so produced match that of the front-end electronics so as to signal reflections are minimised. Another significant consideration is the attenuation of the pickup strips that should be minimised as well. To begin with, we have used pickup panels made of 12 mm thick foam on either side of which aluminum foils are pasted. Pickup strips of about 30 mm are realised by machining the aluminum foil on one side of the composite. The foil on the other side is used as a common reference plane during the signal conditioning by the front-end electronics. The characteristic impedance of these strips is usually about 110. Since the characteristic input impedance of the front-end electronics is 50, this requires use of impedance matching circuits between the pickup strips and front-end electronics. We have also designed and

developed the pickup panels which use G-10 panels which are usually used to fabricate electronic printed circuit boards (PCBs).

Fig 3.3 Fabrication of Pickup Panel for interfacing with front-end electronic

However, based on cost and other considerations, we have developed panel boards made of 5 mm thick foam laminated with aluminum foil on both sides. This was done in collaboration with a local industry. The density of the polyurethane (PUR) foam is 40 kg/m^3. While the aluminum foil is 0.2 mm thick, the adhesive films which bind the foil with the foam is 33 g/m^2 (GSM). These panels were machined to form the pickup strips of required pitch as mentioned above. A number of measurements were carry out to choose the characteristic impedance of the transmission line created by the pickup strip and ground plane, the dielectric constant of the foam and the signal attenuation along the strips.

We have use the experimental set up shown in Figure below to calculate the characteristic impedance of the pickup strip. A waveform generator is used to send a pulse through a 50 m cable. This cable is coordinated to a pair of twisted pair lines of characteristic impedance of 110

using an impedance matching network. While one line goes to an oscilloscope for measurement, the other is connected to the pickup strip whose characteristic impedance we want to find. A variable resistor is connected between the two plates of the pickup and adjusted such that the reflection from the far end disappears. This is the characteristic impedance of the strip. This value can be calculated using the dimensions of the pickup strip and the dielectric constant of the foam material. Our measured values were found to agree well with the calculated values. A typical sequence of signals seen on the oscilloscope for a case of un-terminated strip to the matched termination resistor values are shown in Figure below in clock-wise direction initiating from the leftmost trace. The measurements are done for strips of different widths and at different signal frequencies. We can also estimate the capacitance of the strips and hence the dielectric constant of the foam by using the strip as a capacitor in a mono-shot circuit. We summarized the measurements on characteristic.

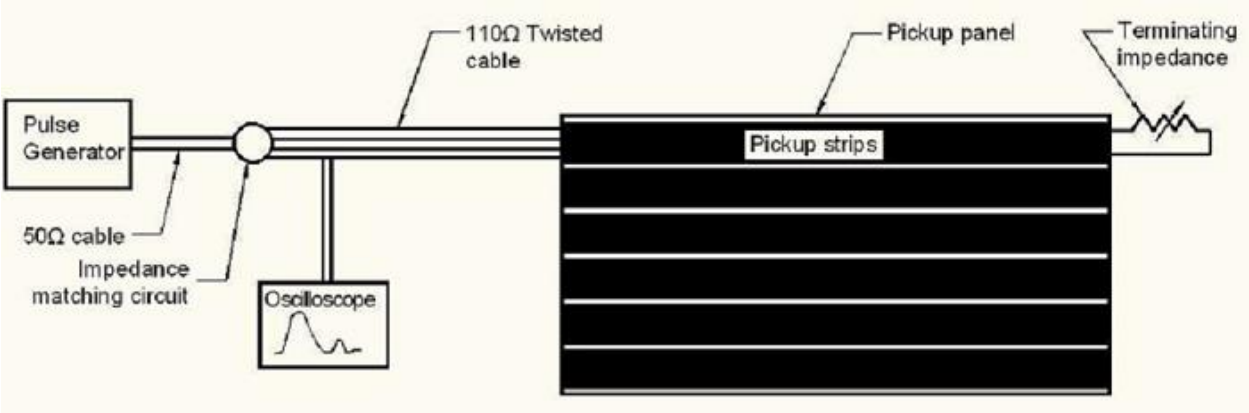

Fig 3.4 Experimental set up for measurement of characteristic impedance of pickup strips

Table 3.1: Summary of characteristic impedance measurements of RPC pickup strips.

Pulse Frequency (KHz)	Z_c (ohm)
4.0	117.1
2.0	114.6
1.33	100.0

Table 3.2: Summary of capacitance measurements of RPC pickup strips.

R_{ext} (Kohm)	t_w (nS)	C_{ext} (pF)
10	283.6	59.1
20	550.0	57.3
30	817.9	56.8
40	1075.3	55.9
80	2162.0	56.1

In addition, there is also a requirement for designing a suitable arrangement for providing mechanical support and rigidity to the RPC detector. When using foam based pickup panels, this requirement is met by designing a box-like structure using aluminum around the RPC. This has resulted in an increase in the thickness of the RPC, in addition to the increased cost of its fabrication.

The design of the ICAL detector structure is carried out assuming a minimum thickness for the active detector elements in order to contain 150 of these layers are as well as to minimise the magnetic field variation inside the structure. Due to the reasons mentioned above, it was decided to work on development of a solution that combines the two functions, namely that of pickup panels and of the support structure for RPCs.

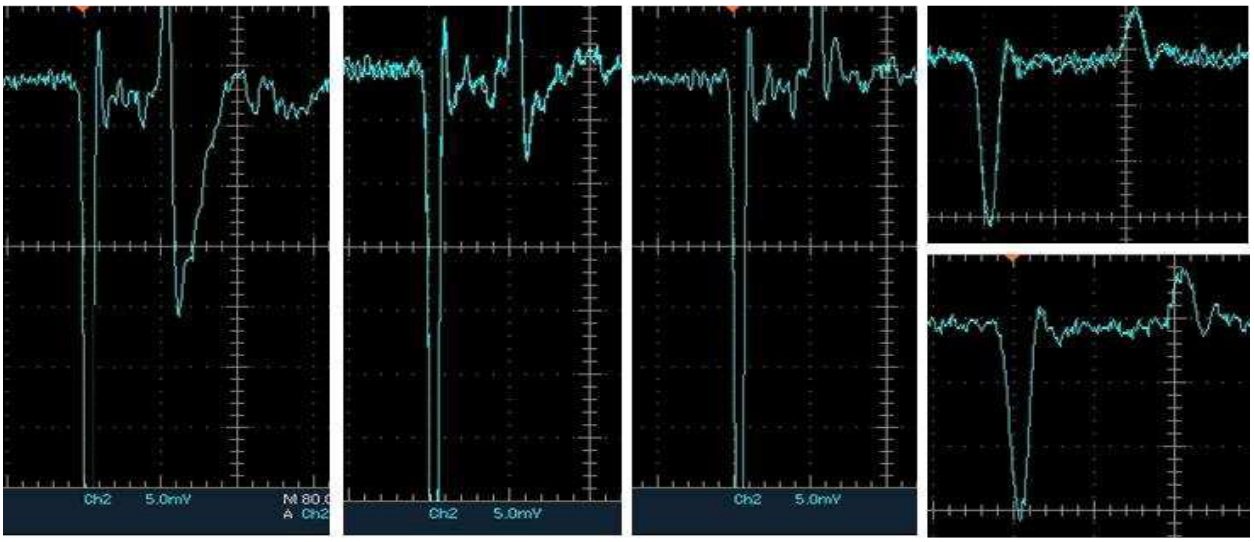

Fig 3.5 Typical signals are seen on oscilloscope during measurement of characteristic impedance of pickup strips. The snapshots from left to right and in clock-wise direction correspond to termination resistances of open, 100, 51, 48.2 and 47 respectively.

We have finally developed plastic honeycomb panels of 5 mm in thickness, laminated on one side by 100 μ m thick aluminum sheet and the other side by 50 μ m thick copper sheet, with the help of a local industry. Pickup strips of 30 mm in width are realised by employing the same machining method on the copper sheet. Aluminum side acts as the signal reference layer. The honeycomb panels were found to be an excellent solution for the mechanical support to the RPC, since it offered better rigidity to the detector with much smaller weight than that of aluminum. The characteristic impedance of these pickup strips turned out to be 500, which has also eliminated the requirement for any impedance matching circuits between the pickup strips and the front end electronics.

3.1.5 DESIGN AND DEVLOPMENT OF RPC CASINGS:

Resistive Plate Chambers are planar geometry detectors. The RPC gas gaps (or volumes) which will be used for the ICAL detector are about 4 m^2 in area, but are only 8 mm thick. This extremely disproportionate and heavy detector module (weighing about 30 kg) poses serious problems in terms of mechanical rigidity and difficulties in the packing, transportation and

Fig 3.6 Honeycomb panel with milled copper pickup strips

installation of the modules in the detector. In addition, in spite of cohering the glass sheets together with a matrix of buttons throughout the area and using spacers on the four edges, the chamber tends to knob outwards when the gas is flown through the chamber. The trouble becomes more severe, in the detector as many modules will be cascaded in series in order to implement the gas flow using minimum number of gas channels and thus increasing differential pressure across the chamber gas ports further. These considerations call for a suitable and lightweight casing for the chamber. In our case, the RPC case in addition to providing the mechanical strength required for the gas gap, will also house the pickup panels, gas and high voltage connections to the chamber as well as various frond-end electronics components. We have designed and tested an aluminum based RPC case to begin with, but could not achieve the desired results in terms of the mechanical strength and other considerations. We subsequently replaced the aluminum panels by aluminum honeycomb panels. This design change seems to have solved the problem and we could achieve all the required results. In order to even improve the mechanical strength further, we have bent the top and bottom panels of the casing with a radius of curvature of 10 mm and mounted the panels in the assembly such a way that the parabolas face outwards. Shown in Figure below is a detector being assembled in a RPC case which was fabricated using the aluminum honeycomb panels.

3.2 DEVLOPMENT OF LARGE AREA RPCs:

Having learnt the science and technology of the RPC design through production and characterization of small prototype chambers, as well as having formed all the materials, process and infrastructure required for detector R&D of ICAL experiment magnitude, we have taken the next logical steps to develop larger area RPCs of 100 cm $\times$ 100 cm in dimensions. We used 3 mm thick Asahi Float glass sheets which were procured locally. We measured its bulk resistivity (ρ) to be 2×1012 -cm. We have essentially used the materials, followed the procedures and utilised the infrastructure described in the previous sections.

The glass sheets were coated with the special paint that we had developed and applied using the automatic plant. The polycarbonate spacers, buttons and gas nozzles were used for the assembly of the gas gap, which was put in place by using the vacuum jig. Machined plastic honeycomb panels mounted orthogonally on each side of the gas gap, were used for signal pickup. Lastly the

chamber was packed inside a case made of aluminum honeycomb panels, a photograph of the fully assembled such RPC along with its efficiency plateau characteristics obtained using a cosmic ray muon telescope. cosmic ray test stand. These chambers were arranged in a detector stack and are in continuous operation now for about two years tracking cosmic ray muons. The data obtained from this detector has help us to improve our sympathetic of the RPC design, characteristics, long-term stability etc.

3.2.1 ASSEMBLY OF 100 cm × 100 cm RPCs

Based on our detector R&D and development of a variety of materials and fabrication process, we have built RPCs of 100 cm× 100 cm in area, which are required for the detector stack. The RPC gas gaps were fabricated using 3 mm thick Asahi Float glass sheets procured from local market. The glass sheets were coated with a semi-resistive paint using an automatic plant. Both the paint and the plant were developed in collaboration with local industries. Polycarbonate buttons, spacers and gas nozzles, which were produced indigenously and fabricated by other local industry, were used to gather the gas gaps. The gaps were fabricate with the help of a pneumatic jig, which ensure that the gap between the glass sheets is consistent all through gas volume as well as all the joints are glued well. Custom built honeycomb panels, build as a compound of plastic core padded on both sides with copper sheets, be used for signal pickup as well as for provide the mechanical inflexibility to the assembled chamber. Two panels, each ridged with 30 mm signal pickup strips were mounted on each side of the gas gap and orthogonal to each other in order to record particle hit coordinates in both X-planes and Y-planes. Polyester film was used to separate the signal pickup panels from the RPC gas gap surfaces, which are maintain at high voltage while the RPC is in process.

Fig 3.7 Assembling of 100 m X 100 m RPC.

Figure shows the mechanical drawings of a base chassis made of aluminum honeycomb panels, on which the RPCs are assembled. The low voltage power supply (for pre-amplifiers) and high voltage (for RPC) as well as the inlet and outlet gas connectors are all terminated on the chassis as shown in the left panel. The right panel shows the placement of an RPC gas gap on the chassis. The front-end preamplifier boards are mounted in the area between the RPC gas gap boundaries and the front and left edges of the chassis. The other two edges of the chassis are sealed along with the top honeycomb panel, using an adhesive aluminum tape in order to provide the necessary electromagnetic induction (EMI) shielding for the assembled chamber. It may be noted that in this design, the preamplifier boards occupy substantial area on the chamber, which essentially amounts to dead space for charge particle detection. However, front-end electronics for the ICAL detector is being designed based on ASICs and the same will be integrated within the RPC foot-print itself.

3.2.2 CONSTRUCTION OF DETECTOR STACK:

We have fabricated a appropriate stand using aluminum/wood sections to house twelve RPCs of 100 cm $\times$ 100 cm in area. The stand facilitates easy insertion, removal and precise alignment of the RPCs to the level of a few mm, which is essential to configure the detector to track cosmic ray muons. The inter-layer gap is fixed at 160 mm. A picture of the stack in operation is shown in Figure. As can be seen in the figure, two multi-level racks built again using aluminum sections, are anchored to either sides of the front-face of the detector stack. All the front-end electronics circuit boards along with the necessary cabling are installed in these racks. This arrangement has helped in reducing the analog signal cable lengths from the on-detector preamplifier boards to the front-end electronics racks and improved the signal fidelity. In addition it offers high flexibility to service the front-end electronics system.

Fig 3.8 Detector stack

3.2.3 POWER SUPPLY AND MONITOR STACK:

The required field across the Resistive Plate Chamber (RPC) glass electrodes is setup by applying a differential high voltage of $\pm$4.9 kV, using contact on the semi-resistive coats. The

chamber current drawn during the operation is typically in the range of 100 nA per RPC. In order to carry out RPC plateau studies and due to other operational reasons, we required a provision of ramping up/down the high voltage at a required step size. Also since the stability of an RPC could be ascertained by its chamber current, a facility to monitor the output supply voltages and load currents - channel-wise, was an essential feature of the high voltage power supply.

The front-end electronics for the detector stack, comprising of preamplifiers, analog and digital front-end sub-systems as well as signal routers, require d.c. power supplies such as ± 6 Volts and ± 8 Volts. Average load currents on these power rails are 25 and 90 Amps for ± 6 Volts and 15 and 25 Amps for ± 8 Volts, respectively. Essential requirements of the low voltage power supply system are fine control of supply voltages at the load points and the monitoring of supply voltages and load currents.

Both the power supply systems were designed using commercial components from CAEN and shown in Figure. The high voltage system comprises of two twelve channel high voltage supply modules - one each for either polarity, plugged into an SY2527 power supply mainframe (shown in the left panel in the figure). The low voltage power supply system similarly comprises of several supply modules, plugged into an Easy system crate. The 48 volts raw d.c. power is supplied to the Easy system using a 3-phase AC/DC converter. The system is controlled and connected to the SY1527 mainframe, through a branch controller installed in the latter.

Based on the power supply requirements of individual front-end electronics modules, a suitable scheme was designed to distribute power from the power supplies to various modules. Multiple bus-bars made of thick copper strips were used for this purpose so that the Ohmic voltage drops across the connecting conductors could be minimised. While the input power lines from the power supplies were connected on one end of these bus-bars, power supplies needed by various front-end boards were directly tapped from these bus-bars. This bus-bar based low voltage power supply distribution design has also resulted in improved ground quality to the electronics and data acquisition system.

Both the low voltage and high voltage power supply systems support control and monitoring of various parameters and values through Ethernet ports. We have developed a comprehensive PC based software system on this interface, using which the required voltages are set on various

output supply channels. The set voltages and load currents are logged in on round the clock basis, which are used to correlate them with long-term behaviour of the RPCs along with ambient conditions etc. Typical screen shots of low voltage and high voltage power supply system monitor consoles are given in Figure.

Fast preamplifiers

The RPC signal pickup strips which are realised by milling the plastic honeycomb based panels were characterised and found to offer a characteristic impedance of 50. In the avalanche mode of operation, in which we chose to run the RPCs for ICAL, typical signal range on these strips across a 50 load is 0.5 - 2 mV and rise time of about 1 ns. Hence, there is a need for a high speed, low noise pre-amplification for the RPC strip signals before it can be further processed by the front-end electronics. We extract these signals into the front-end electronics by terminating the far-end of the strip by a 50 resistor and connecting the near end to a 8-in-1 two-stage Hybrid Micro Circuits (HMC) based high speed high gain preamplifiers. Two types (BMC 1595 and BMC 1597) of first stage HMCs - one of each for positive and negative polarity strip signals, were designed to provide a nominal gain of 10 and a negative polarity output signal. The second stage HMC (BMC 1513) offers another factor of 10 gains to these signals. All these HMCs1 share similar design characteristics, such as input signal handing range (100 - 200 mV), bandwidth (350 MHz), rise time (2 ns), power rails ($\pm$6 Volts) and power dissipation (120 - 140mW). Shown excellent performance, matching to the design parameters. As can be seen, all the eight channels of the board show a uniform gain of about 90 over a broad range of input signals. The preamplifier boards are fitted inside a galvanised iron (GI) mounting case before installing in the RPC chassis in order to improve the EMI shielding as well as grounding especially at the input side of the board.

Front-end electronics

The Time-of-Flight array for the ALICE experiment will be built using Multi-gap Resistive Plate Chambers (MRPC) in the form of strips, each with an active area of 1:2m-7:4 cm, read out with 96 readout pads of 2:5 -3:7 cm^2 area. Since exceptional time precision is needed, small gas gaps (250 mm width) are employed; to reach maximum efficiency 10 gas gaps are used, arranged in a double stack as revealed schematically. It should be noted that with this design every cell has a

single anode readout pad and two identical cathode readout pads. As the coupling between the movements of charge in any of the ten gas gaps to the pickup electrodes is the similar, the induced signal will be the sum of signals from the gas avalanches occurring in some of the gaps. Due to the thin gap, the induced signal will be formed 500 ps after the passage of the through-going charged particles and have rise time of some hundreds of ps. The reason for building the detector as a strip is of two-fold. One cause is that the strips can be tilted so that the detector plane is normal to incoming particles in the XY plane; thus the surface of the pickup pad is a plane at a fixed distance from the interaction point (therefore the time of arrival does not depend on the collision point). The other reason is that it allow the readout of both anode and cathode pad, therefore derive a differential signal from the detector. Firstly we had tried to building a planar device reading out the anode pads on the one side with the return path to the cathode pads during the metallic box of the detector.

3.3 DESIGN OF THE NINO ASIC

The NINO ASIC have to fullfill the following requirements:

(1) Differential input;

(2) Optimized to operate with 30 pF input capacitance;

(3) LVDS output;

(4) Output pulse width dependent on the charge of the input signal (need not be a linear dependence);

(5) Fast amplifier to minimise time jitter, i.e. first stage with a peaking time of 1 ns;

(6) Threshold of discriminator adjustable in the range 10–100 fC;

(7) Eight channels per ASIC. The intend design of the circuit was outsourced. The layout was done at CERN and submitted as part of a MPW run to IBM (0:25 mm CMOS).

The NINO amplifier-discriminator architecture was first developed in order to read out Multigap Resistive Plate Chambers (MRPC) in the ALICE Time-Of-Flight (TOF) detector at CERN. Particle identification is made in this detector by measuring the Time-Of-Flight of the high-

energy incident particle with the resolution better than 100 ps. When a particle goes through a MRPC channel, a current signal in the sub-ns range is generated on the channel electrodes and this information has then to be readout with high timing precision electronics. The NINO circuit was developed in a 250 nm CMOS technology as front-end readout of the MRPC detectors. Each MRPC channel is differential and is connected to one differential channel of a NINO chip. The NINO chip developed for this application integrates 8 channels and is presented in Figure.

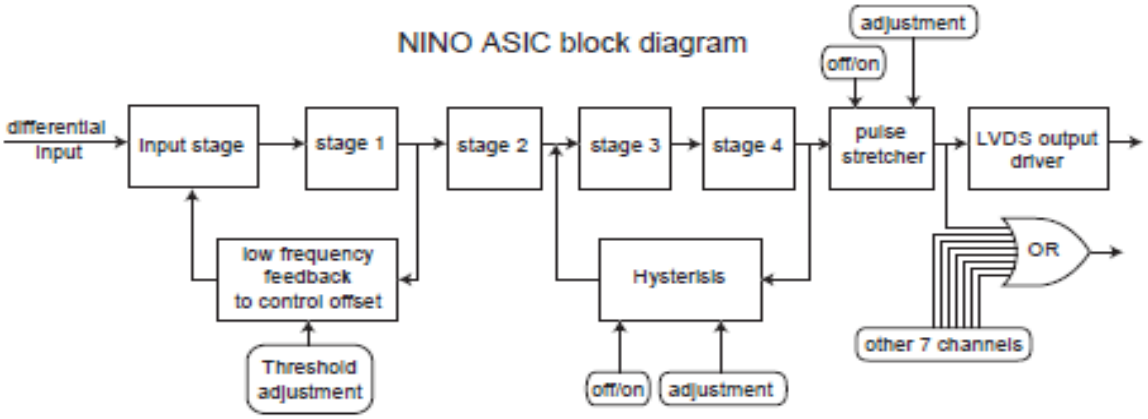

Fig 3.9 Block Diagram of NINO ASIC

Each channel is a fully differential ultra-fast (< 1 ns peaking time) preamplifier discriminator with a minimum detection threshold which can be adjusted from 10 to 100 fC for input current shapes in the ns range. The architecture is presented in Figure. An input stage permits a fast current to voltage conversion and presents low input impedance (which can be adjusted from 30 to 100 Ω). Voltage gain amplification is then provided with four cascaded identical large bandwidth differential pair amplifiers (each amplifier has a voltage gain of ~ 6, with – 3dB around 500 MHz). Saturation of the signal permits to have voltage pulse information at the output of the circuit (the pulse width thus varies as a function of the total input charge). A further block permits to set a threshold for the differential amplifiers and to perform compensation of eventual offset. The design of a NINO channel thus comprises optimization of the input stage (for speed, primary gain and input impedance), optimization of the cascaded differential amplifiers (for speed, gain and output signal levels) and optimization of the feedback block which sets threshold level and performs compensation.

The NINO circuit also integrates two additional blocks which can be set active or passive from outside the circuit: a hysteresis circuit and a stretcher. The hysteresis circuit is a feedback loop placed between the outputs of the 4th and 2nd differential stages. It permits to have discrimination level different for rising and falling edges of the comparator (forces hysteresis: different $V_{th}$for rising and falling edges). This permits to cure eventual comparator instability. The stretcher is a circuit placed between the 4th differential stage and the driver. It permits to stretch the output pulse width, so that by default minimum pulse width is at about 13 ns. This permits to use the NINO circuit together with the HPTDC chip developed at CERN, which can perform timing measurement every ~ 10 ns only. Using the stretcher permits to do both the measurements of the leading and trailing edges. The full architecture is presented in Figure.

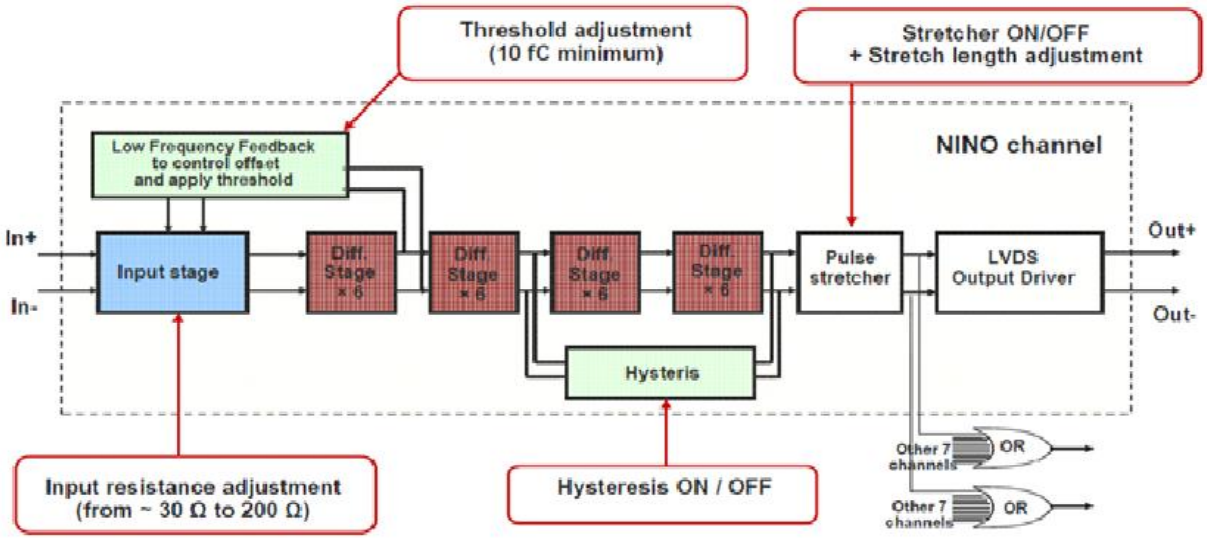

Fig 3.10 Schematic Diagram of NNO ASIC Chip.

The circuit has been earlier discussed. The detector is connected to the input of the NINO ASIC Chip with a short transmission line; therefore the input impedances has to match the transmission lines and an open loop current to the voltage conversion (no feedback) should be used. The circuit as shown in Figure to satisfies these requirements. The input current pulse is feed into the sources of the NMOS (M1) transistor, emerge from the drain and is again fed into the source of the second NMOS (M2) transistor. The current pulse will then emerge from the drain of M2, but the impedance at this point is extremely different (much better) than at the input. This current charges the capacitance (which is the inescapable stray capacitance related with the transistor) on

the drain; the rise time of this signal is govern by the characteristics of the transistor itself while the fall time is known by the time the capacitance C takes to be recharged (i.e. RC). The input impedance and so the biasing and geometry of M1 is chosen to keep this impedance low to match the transmission line carrying the input signal. The output voltage is definite by the parasitic capacitance C and thus the M2 is designed to minimise this capacitance.

A block diagram of the NINO is shown in Figure. The input stage is followed by 4 stages of low-gain, high-bandwidth differential amplifier. A slow feedback circuit supplies the current to make sure that the input stages stay correctly biased. In addition to an offset is added at this point so as to acts as a threshold adjustment. There is a stretcher just before the LVDS output driver. The pulse width before stretching vary between 2 nano-second and 7 nano-second; the HPTDC that will be used in ALICE can only calculate both leading and trailing edges of an input pulse for width greater than 6 nano-second; thus the pulse stretcher will increase the pulse width by 10 nano-second.

3.4.1 CHIP DISCRIPTION:

The NINO amplifier and discriminator chip has been fabricated for the precision time measurement required for detectors like the in ALICE Time-of-Flight experiment. The present chip has eight channels with a peaking time of 1ns with a resolution of 20 ps rms. Pulse width measurement is used to do charge measurement as well as time walk correction. The threshold can be fix at 10 fC input charges. The power consumption per channel is 30mW, including the LVDS compatible output driver. Only one power supply, two external resistors and a differential voltage source are needed to make the circuit operational.

The amplifier has differential inputs with tunable input low impedance. The input impedance is defined by value of external resistances REXT. The signal after discrimination is differential LVDS level, with a delay time as short as 1ns and a pulse width in the range of 3 to 10ns (Stretcher OFF) or 13 to 20 ns (Stretcher ON). The pulse width measurement through a precision TDC can be used to measure the input signal charge and compensate for the time walk. Very low jitter has been characterized on this chip. A Hysteresis Control can be used to add an hysteresis to the discrimination function, at the cost of an increase of the jitter in the output signal. The

discrimination level is set by the two differential signals VTH+/-. The threshold range can be selected in the range of 10 to 100fC with a ratio of approx. 10mV/fC.

Power supplies:

The NINO chip requires 2.5V nominal power supplies connected between VDD and VSS pins (output drivers current) and between VDDA and VSSA pins (analogue channels current). The VSS and VSSA have an ohmic connection on the chip, whereas VDD and VDDA are independent. The VSSA and VDDA power lines should be made as quiet as possible. Separate power sources or separate filtering on VDD and VDDA are recommended.

Channels Input and Outputs

Each of the eight channels has two differential inputs (inM and inP) and 2 differential LVDS level outputs are (OUTM and OUTP). Detector signal should be flowing between the 2 low impedance inputs. The differential impedances are matched to the REXT external resistors value. REXT can be tune in the range of 30 to 70 ohms. The input voltages are set internally in the NINO: therefore the detector should be seen as a high impedance current source or capacitive coupled to the input nodes.

The differential outputs (i.e. OUTM and OUTP) are current mode LVDS compatible outputs : the current is set by the resistor on bias input BiasN6 and his supposedly 6mA. Loaded with 100 ohms the differential voltage of the outputs is +/-300mV.

Special care should be taken on the PCB layout to separate the inputs lines from outputs and others lines. The input lines should be as short as possible, isolated and symmetrical to maintain the input impedance matching.

Biasing inputs

A resistor REXT has to be set between the 2 inputs RextPlus and RextMinus : the differential input impedances are matched by circuit to the value of this resistor, in the range of 30 to 70 ohms.

A resistor has to be connected between VDD and the input BiasN6 to find out the LVDS driver output current. Typically 200 ohms will deliver 6mA differential current capability per channel.

The pins labeled BiasN5, BiasN7, and BiasN8 should be left unconnected or attached to a decoupling capacitor to VSSA on PCB.

Threshold setting

TH-Plus and TH-Minus should be connected to a circuit that provides a reference differential voltage that sets the internal discriminator threshold, with the approximate ratio of 10mV/fC. The DC level of these 2 signals should be between 1 and 1.4V.

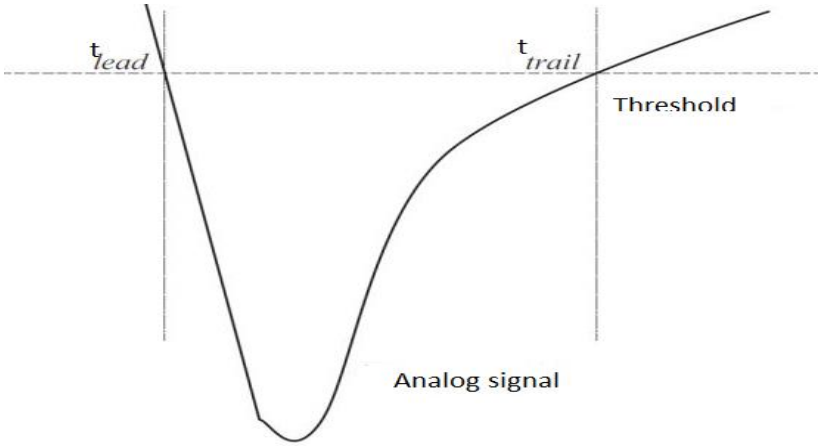

Fig 3.11 Block Diagram of Threshold

WO+/WO- Outputs

The differential ouputs (WO+ and WO-) are current mode LVDS compatible outputs: they deliver a differential signal when any of the 8 channels has received an input signal that goes beyond the threshold. The pulse duration of the same magnitude has for the channel signal, however these outputs cannot be used for precise time measurement.

Hystoff and StchOff

The characteristics of the channels outputs are depend on the logic (DC) values of the Hystoff and Stchoff inputs:

- With the default setting of 0 (VSSA, pull down on chip), the Hysteresis circuit and the Stretcher circuit are enable.
- If Hystoff is wired to 1 (VDDA) : The Hysteresis circuit is OFF.
- If Stchoff is wired to 1 (VDDA) : The pulse length stretcher circuit is OFF.

The output pulse length is between 3 and 13 nano-second when Stchoff is set to 1, and between 13 and 23 nano-second when Stchoff is set to 0.

The activation of the Hysteresis circuit may help to minimally discriminate detector signals but has negative effects on the output signal time jitter.

3.4.2 Package Information

Table 3.3: Pin Package Distribution

PIN NAME	PIN NUMBER
VSSA	B13
HystOff	A16
StchOff	A17
BiasN8	A18
VDDA	B14
VDDA	B15
WO+	A19
WO-	A20
VDD	B16
VSS	NC
VSSA	NC
InM8	B11
InP7	B10
VSSA	B9
InM7	A13
InP7	A12
VSSA	B8

InM6	A11
InP6	A10
VSSA	B7
InM5	A9
InP5	A8
RextPlus	A7
RextMinus	A6
InM4	A5
InP4	A4
VSSA	B5
InM3	A3
InP3	A2
VSSA	B4
InM2	A1
InM2	A44
VSSA	B3
InM1	B2
InP1	B1
VSSA	NC
VSSA	B31
ThPlus	A41
ThMinus	A40
BiasN7	A39
VDDA	B30
VDDA	B29
BiasN5	A38
BiasN6	A37
VDD VSS VSS	NC B28 NC

OUTP8	B17
OUTM8	A22
VSS	B19
OUTP7	A23
OUTM7	A24
VDD	B20
OUTP6	A25
OUTM6	A26
VSS	B21
OUTP5	A27
OUTM5	A28
VDD	B23
VSS	B24
OUTP4	A29
OUTM4	A30
VDD	B25
OUYP3	A31
OUTM3	A32
GND	B26
OUTP2	A33
OUTM2	A34
VDD	B27
OUTP1	A35
OUTM1	B27
VDD	NC

CHAPTER 4

RESULTS AND DISCUSSIONS

SETUP:

The signal coming from the detector is amplified by the NINO ASIC chip so that the charge and corresponding width can be calculated. The path of the pulse is shown in figure. The signal coming from the detector is simulated as a Gaussian function with amplitude 20-60mV (333fC 1000fC on 50 Ohm resistor) and variance 0.33ns. This gives a 2 ns signal.

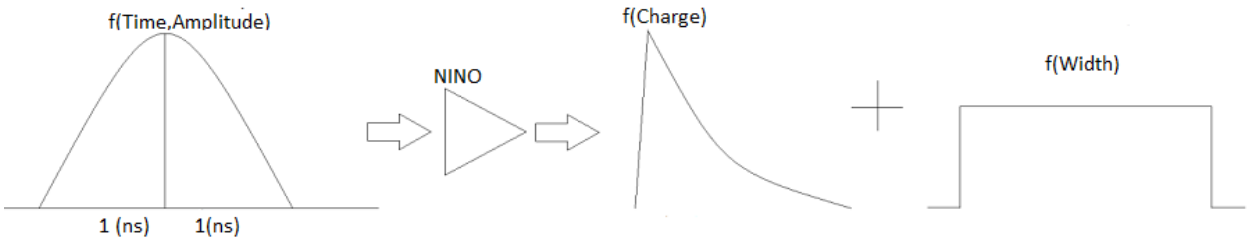

Fig 4.1: The pulse coming from the detector and going through the NINO chip

The charge of the pulse is the area beneath the pulse. The width of the pulse is then calculated by the parameterized functions of Figure. In order to find the parameterized function of figure it was fit with three different functions as shown in Figure.

- 0−100 $width = -3.5 + 0.17 \times charge$
- 100−200 $width = 8.4882 + 1.0919 \times \log(charge)$
- 200−1200 $width = 13.824 + 0.0016182 \times charge$

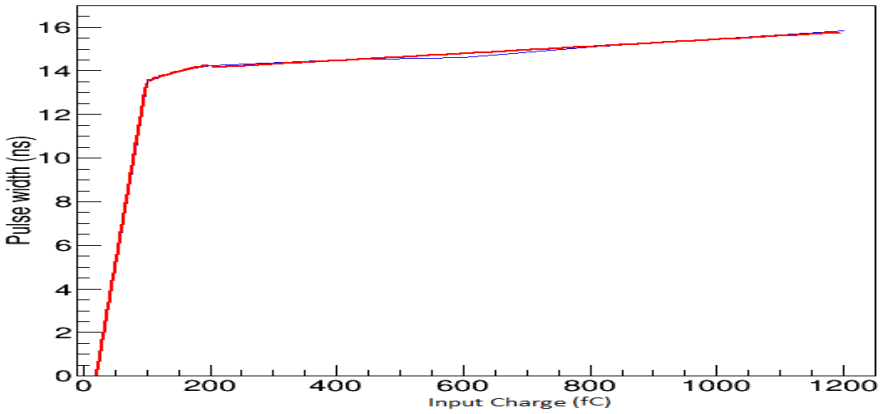

Fig 4.2 Fit of input charge with the pulse width

Once the width has been calculated the time of the pulse can be calculated through:

$$time = 74.664 * \exp(width/2.6315) - 0.23854$$

The time and width of a pulse related to this equation is shown in figure.

Calculating the difference between the signal with and without noise the time distribution can be measured. Two different types of noise was considered, sinusoidal based noise and Gaussian white noise, as shown in Figure below,

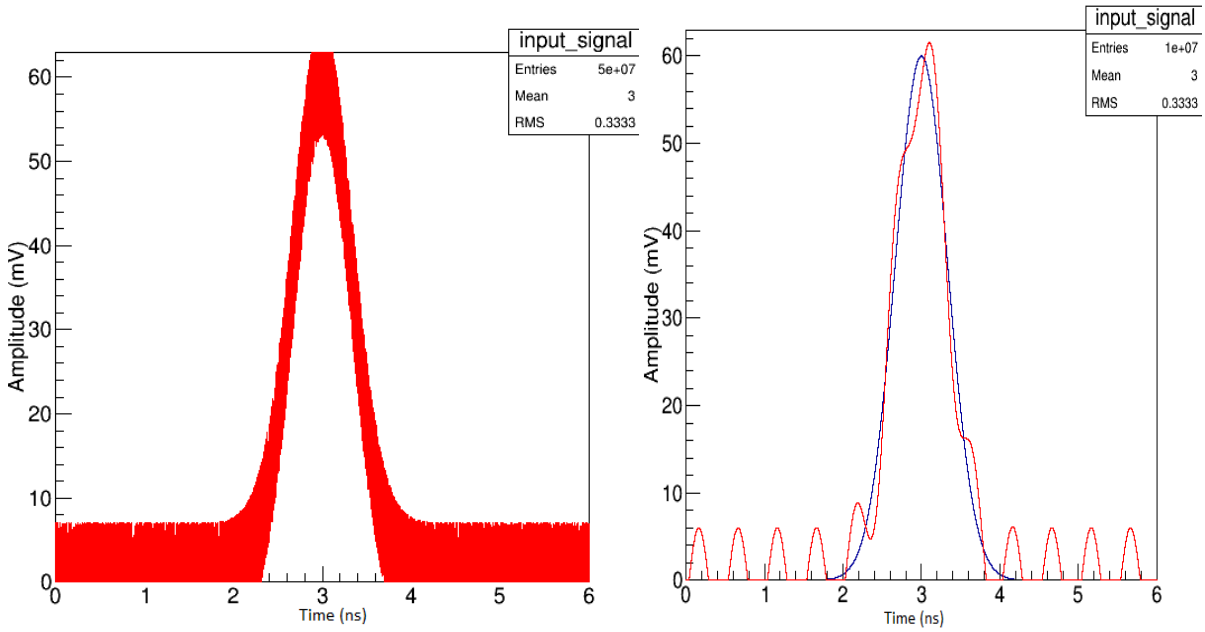

Fig 4.3 An example of Gaussian white noise (left) and sinusoidal noise (right)

The sinusoidal noise was defined as:

$$y = A \times \sin(2\pi f + \phi/2)$$

Where A is the amplitude of the noise, f the frequency and ϕ the phase. The white noise was generated using the box-muller method. The box-muller method uses inverse transformation to turn 2 uniformly distributed random numbers into 2 unit normal random numbers with mean 0 and variance 1.

$$y_1 = \sqrt{-2}\log(R_1) \times \cos(2\pi R_2)$$

$$y_2 = \sqrt{-2}\log(R_1) \times \sin(2\pi R_2)$$

Where R_1 and R_1 are two uniformly distributed random numbers and $R_1 \neq 0$. The mean and variance can easily be modified by:

$$y_1' = mean + \sqrt{variance}\, y_1$$

The frequency, phase, signal and noise amplitude is varied respectively and the effect this has on the width and time distribution is studied. When the parameters are not varied they are kept constant at:

- Resistance at 50Ω.
- Signal amplitude at 60mV (charge at 1000fC).
- Noise amplitude at 10% of signal amplitude.
- Phase at 0ns.
- Frequency at 2GHz

EXPERIMENTAL SETUP:

Using a signal generator (A) a two ns Gaussian signal is generated. This signal is then split into two parts, one part going to the oscilloscope (E) and the other part going to the differential splitter (G). The differential splitter has one input channel and four output channels. Normally the differential splitter takes the input signal and produces four similar signals of which two is positive and two negative. The amplitude of the output pulses depends on the power supply (C) of this circuit. When the pulse from the sinusoidal noise generator (D) is attached to the power

supply, the amplitude of the output signal is changed according to the sinusoidal pulse, thus adding the noise to the signal. This is shown in the figure.

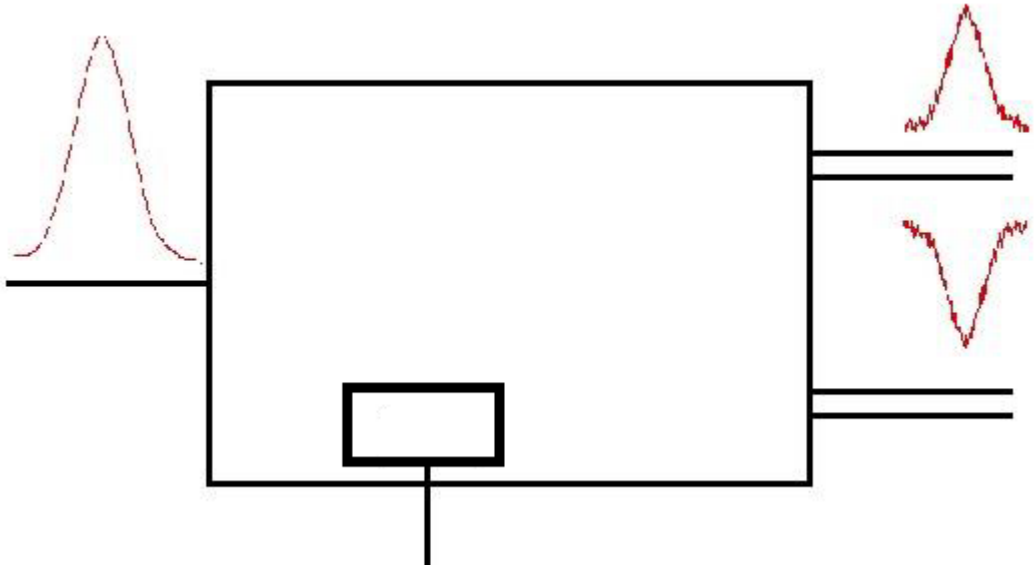

Fig 4.5: Diagram of the differential splitter

Two of the signals from the differential splitter go directly to the oscilloscope, and the other two goes to the NINO amplifier and then the oscilloscope. A diagram of the setup is shown in Figure and pictures of the setup is shown in figure

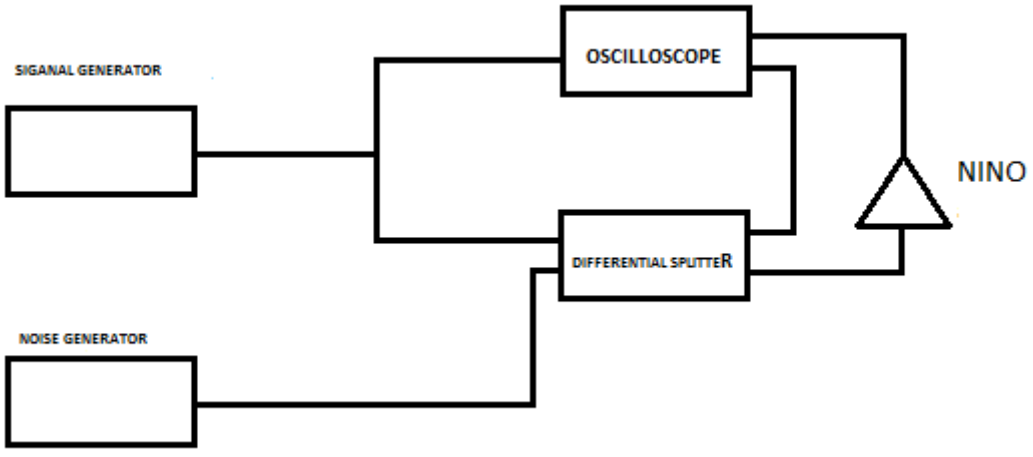

Fig 4.6: Diagram of the experimental setup

Using this setup data is taken with varying noise amplitude from 100-1000mV (where 100mV is 10% of the signal amplitude) and a constant frequency of 1GHz. Data is also taken with varying frequency from 0MHz to 1GHz with a constant noise amplitude of 100mV

Data analysis method

The figure shows the different signals generated. The red signal is the primary signal with noise, and the yellow signal is the primary signal without noise. The integral of these signals is related to the charge produced in the MRPC by a charged particle. The green and blue signals are the signals coming from the NINO amplifier. The width of these signals is related to the charge from the RPC.

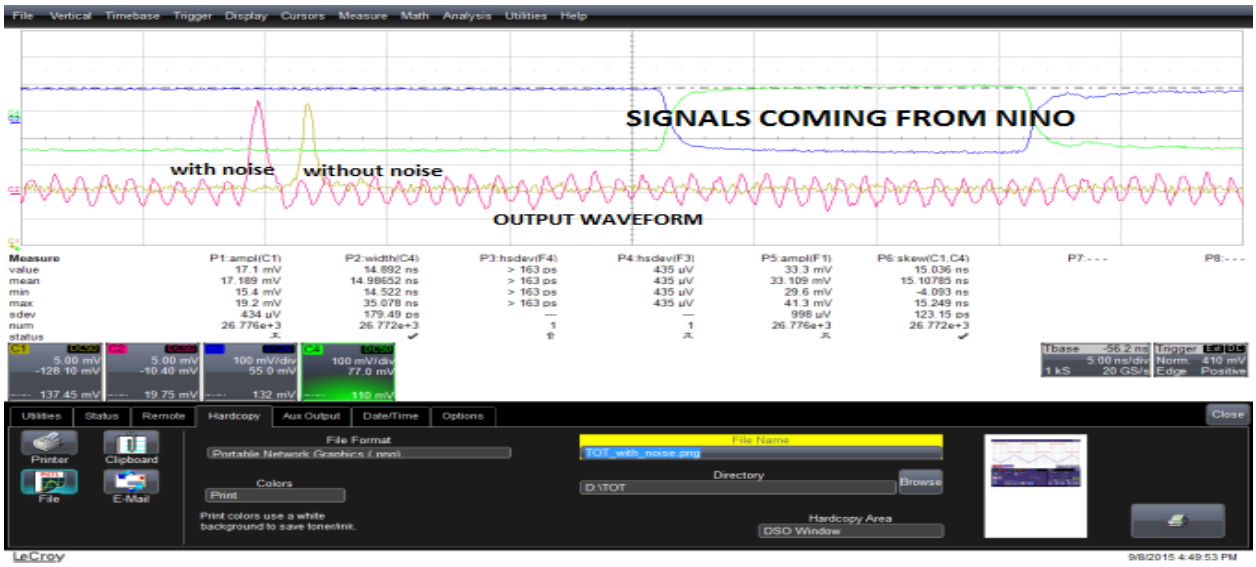

Fig 4.7 The different signals investigated: the primary signal without noise (yellow), the primary signal with noise (red) and the signals coming from the NINO amplifier (green and blue).

Traces of these signals are used for data analysis. To find the time distribution off the data 3 fits where taken as shown in Figure 26. The start time is found on the signal without noise when the fit of the leading edge (function 2) and the fit of the baseline (function 1) cross. The stop time is found on either of the pulses coming from the NINO amplifier when the fit of the leading edge (function 3) goes through zero.

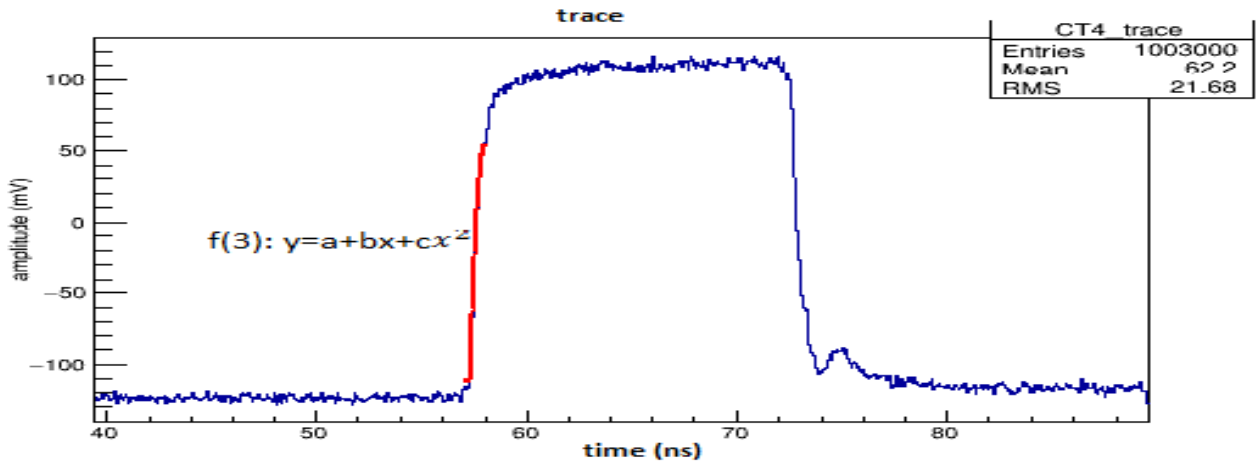

Fig 4.8 Fits for time correction to determine the start and stop time

CHAPTER 5

CONCLUSION AND SUMMARY

Experimentally the NINO amplifier was unstable for all frequencies below 400MHz. The maximum variance introduced by the NINO amplifier and differential splitter is 76ps at 450MHz, while the noise is only 16ps at 450MHz according to the simulation. The variance introduced by the noise seems to be small in comparison to the variance introduced by the NINO amplifier and differential splitter, however, due to the high time jitter (37ps) of the differential splitter, this result has a high uncertainty. A different way of coupling the noise to the signal should be used to experimentally confirm this.

In future we can try to interface NINO to RPC using THS4520 Differential OP-AMP using both passive and active circuits. We can also try to design LVDS/NIM-ECL Translator. The LVDS–ECL translator is designed by using two IC's and interfacing to each other on PCB or Bread Board for desired output.

1. DS90C032B (LVDS- TTL converter)

2. MC 10H124 (TTL-ECL) converter.

LITERATURE CITED

[1] R.Santonico and R.Cardarelli, Nucl. Instr. and Meth. 187 (1981)377-380.

[2] M. Abbrescia et al., "Resistive Plate Chambers in avalanche mode: a comparison between model predictions and experimental results", in Proceedings of the 7th Meeting on Advanced Detectors, La Biodola, Italy, 25-31 May 1997.

[3] INO collaboration 2006 India-based Neutrino Observatory report, INO-2006-01

[4] M C Gonzalez-Gracia, Physics of the Dark Universe 41-5. (2014).

[5] B. Pontecorvo, Sov. Phys. JETP 26, 984 (1968) [Zh. Eksp. Teor. Fiz 53, 1717 (1967)].

[6] Z. Maki, M. Nakagawa and S. Sakata, Prog. Theor. Phys. 28, 870 (1962).

[7] The Technical Design Report of INO-ICAL Detector (2006),http://www.ino.tifr.res.in/ino/.

[8] D. Casper, Nucl.Phys. Proc.Suppl. 112, 161 (2002)[arXiv:hepph/0208030].

[9] A. Chatterjee et al. [arXiv:1405.7243v1][physics.insdet](2014).

[10] M. M. Devi et al., JINST 8 P11003 (2013).

[11] S. Bhide et al. 2007 Preliminary results from India-based Neutrino Observatory detector R&D programme Pramana, Journal of Physics 69 1015

[12] M. Honda et al., Phys. Rev. D70, 043008 (2004)[arXiv:astroph/0404457].

[13] T. Thakore et al. JHEP 05, 058 (2013).

[14] A. Ghosh et al., JHEP 04, 009 (2013).

[15] M. C. Gonzalez-Garcia, M. Maltoni et al, Phys.Rev. D70, 033010 (2004) [arXiv:0404085v1][hep-ph].

[16] ALICE Collaboration, Addendum to the Technical Design Report of the Time of Flight System, CERN/LHCC 2002- 016, Addendum to ALICE TDR 8, 24 April 2002.

[17] ALICE Collaboration, Time of Flight System, Technical Design Report, CERN/LHCC 2000-012 ALICE TDR 8, 16 February 2000.

[18] M. Mota, J. Christiansen, S. Debieux, V. Ryjov, P. Moreira, A. Marchioro, A flexible multi-channel high-resolution time-to-digital converter ASIC, in: IEEE Nuclear Science Symposium, Lyon, France, 15–20 October 2000, p. 9 /155-9/ 159 (v.2).

[19] F. Anghinolfi, P. Jarron, F. Krummenacher, M.C.S. Williams, E. Usenko, NINO, an ultra-fast, low-power, front-end amplifier discriminator for the Time-Of-Flight experiment in ALICE; presented at 2003 Nuclear Science Symposium, Portland, Oregon.

[20] E. Cerron-Zeballos, I. Crotty, D. Hatzifotiadou, J. Lamas-Valverde, S. Neupane, M. C. S. Williams, and A. Zichichi, "A new type of resistive plate chamber: The multigap RPC," Nucl. Instrum. Methods Phys. Res., vol. A 374, pp. 132–136, 1996.

[21] A. V. Akindinov, F. Anselmo, M. Basile, E. Cerron-Zeballos, L. Cifarelli, F. Cindolo, F. J. Choi, B. Cozzoni, A. De Caro, S. De Pasquale, D. W. Kim, N. Y. Kim, W. Klempt, A. Kluge, G. Laurenti, S. C. Lee, V. Golovine, D. Hatzifotiadou, A. N. Martemyanov, P. Martinengo, A. Pesci, E. D. Platner, J. Roberts, A. Seganti, A. A. Semak, A. I. Smirnitskii, M. Spegel, P. Szymanski, G. Valenti, D. Vicinanza, M. C. S. Williams, and A. Zichichi, "The multigap resistive plate chamber as a time-of-flight detector," Nucl. Instrum. Methods Phys. Res., vol. A456, pp. 16–22, 2000.

[22] V. Radeka, "Low-noise techniques in detectors," Ann. Rev. Part. Sci., vol. 38, pp. 217–277, 1988.

[23] Giovanni.Anelli@cern.ch cern.ch/knowledgetransfer.

[24] F. Anghinolfi et al., NINO: an ultra-fast and low-power front-end amplifier/discriminator ASIC designed for the multigap resistive plate chamber, Nucl. Instrum. Meth. A 533 (2004) 183.

[25] ALICE-TOF group and P. Antonioli., The ALICE time of flight system, Nucl. Phys. Proc. Suppl. B 125 (2003) 193.